(NASA-CR-163387) FIBER RING OPTICAL GYROSCOPE (FROG) Final Report (Utah Univ.) 62 p HC A04/MF A01 CSCL 14B

N80-28690

Unclas
G3/35 28296

FIBER RING OPTICAL GYROSCOPE (FROG)

FINAL REPORT

CONTRACT NAS7-100
TASK ND-156
JPL 954936

Prepared by:

Geospace Sciences Laboratory
University of Utah Research Institute
420 Chipeta Way, Suite 160
Salt Lake City, Utah 84108

Prepared for:

Jet Propulsion Laboratory
4800 Oak Grove Drive
Pasadena, California 91103

December 31, 1979

This work was performed for the Jet Propulsion Laboratory, California Institute of Technology, sponsored by the National Aeronautics and Space Administration under Contract NAS7-100.

Geospace Sciences Laboratory Publication 79-014

Participants in this research were:

V. Vali (Physicist)	12-20-77 to 05-03-78
R. W. Shorthill (Physicist)	12-20-77 to 06-39-79
M. F. Berg (Engineer)	12-20-77 to 05-19-78
G. J. Morris (Physicist)	12-20-77 to 06-30-79
L. D. Weaver (Physicist)	07-05-78 to 06-30-79
R. E. McCain (Res. Assoc.)	06-26-78 to 06-30-79

This report contains information prepared by the Geospace Sciences Laboratory, University of Utah Research Institute, under a JPL subcontract. Its content is not necessarily endorsed by the Jet Propulsion Laboratory, California Institute of Technology, or the National Aeronautics and Space Administration.

Abstract

A one meter diameter fiber ring optical gyro using one and one-half kilometers of single mode fiber was constructed. The various noise components: electronic, thermal, mechanical, and optical, wer evaluated. Both DC and AC methods were used. An attempt was made to measure the earth rotation rate (the result was questionable). Polarization properties of the fibers were measured. The construction, design, testing and evaluation are described. It was concluded that fiber ring optical gyroscopes using all discrete components have many serious problems that can only be overcome by discarding the discrete approach and adapting an all integrated optic technique that has the laser source, modulator, detector, beamsplitters, bias element, etc., on a single chip.

TABLE OF CONTENTS

LIST OF FIGURES

1.0 INTRODUCTION

This final report covers the period December 12, 1977 to June 30, 1979. The research was done at the Geospace Sciences Laboratory of the University of Utah Research Institute, Salt Lake City, Utah. A list of those who participated in this research are shown on page *ii*. The design, construction, evaluation, etc., of a Fiber Ring Optical Gyroscope (FROG) are described in the report.

1.1 Purpose

Sagnac interferometers have not been considered for guidance applications because of the lack of sensitivity compared to the ring-laser gyros and certain mechanical gyros. However, the sensitivity of a Sagnac interferometer can be improved by circumscribing an area many times using optical fibers. Several Sagnac fiber interferometers have been made but no systematic study of performance has been done. It was the purpose of this study to evaluate some of the characteristics of the Fiber Ring Optical Gyroscope using one kilometer or more of optical fiber. Polarization effects, intensity variations, and reflections are some of the optical characteristics that were studied. Mechanical motion of the fiber holders and thermal variations are examples of other characteristics observed during the evaluation of the system. An attempt was made to detect earth rotation. The results were questionable, however, because of the optical and electronic noise present during the measurement.

1.2 The Optical Gyroscope

The first optical gyroscope was built in 1913 by Sagnac[1]. In this instrument, an area A = 866 cm^2 was circumscribed by oppositely traveling light (mercury light) beams. The rotation rate was 2 revolutions/sec. A shift of

0.07 fringes were observed. At that time, the readout accuracy was about 0.01 fringes. These results were consistent with the expected value, but the accuracy was marginal. The experiment was repeated by Pogany[2] in 1926, with an area A = 1178 cm^2 and an angular velocity of 157 rad/sec. He reproduced the theoretically expected value within 2%. In 1925, Michelson and Gale[3] detected the rotation of the earth by means of the optical gyroscope. The area in this case was a rectangle of 640 x 320 meters.

These and other related experiments showed that the fringe shift ΔZ, 1) obeys the formula $\Delta Z = \frac{4\omega A}{\lambda c}$, where ω is the rotation velocity, A is the enclosed loop area, λ is the free space wavelength of light, and c is the free space velocity of light; 2) does not depend on the shape of the surface area A; 3) does not depend on the location of the center of rotation ω; and 4) does not depend on the presence of a co-moving refracting medium in the beam path[4].

One of the recent configurations of the Sagnac devices is called a "Ring-Laser". It has successfully been used in a navigator. The accuracy of the ring-laser gyroscope has been reported to be at least as good as 0.017°/hr. The ring-laser gyroscope measures the beat frequency between oppositely traveling optical waves in a closed loop laser cavity. The cavity looks longer for the waves traveling in the direction of rotation and shorter for the oppositely traveling waves producing a frequency difference between the counterrotating beams. This frequency difference appears as a beat frequency in the output proportional to the rotation velocity. There are three different types of errors that appear: A null-shift error which arises when the laser cavity is anistropic with respect to the light traveling in the cavity. Gas flow due to discharge current with the associated Fresnel drag, Faraday effect in the gas, etc., can cause the anisotropy. Mode pulling effects are caused by the changes in the scale factor of the gyroscopes. Lock-in which occurs at small beat

frequencies (small angular velocities) makes the beat frequency equal to zero before the angular velocity becomes zero. This is due to coupling between the oppositely traveling waves. The effects of lock-in, for example, can be minimized by dithering.

Some of the problems with the ring-laser can be eliminated when the laser is outside the ring (i.e., when the rotation sensor is a ring interferometer). In general, the sensitivity of a ring interferometer is lower than the ring-laser, but unlike the ring-laser can be increased several orders of magnitude by making the light beam travel around the loop many times. The sensitivity for the interferometer can thus be increased without accompanying pulling, lock-in, and zero shifts.

It is, however, difficult to direct the light beams around an area many times when the beam path is in air or in vacuum. For multiple round trips, mirrors would have to be large or various optical devices would have to be used to maintain the small beam size. Some of the difficulties are removed by using optical fiber waveguide to form the beam path.

An initial effort was carried out under NASA, ONR, and NSF sponsorship to study the physics of interferometers using optical fiber waveguides. It was first shown that the wavefronts remain well defined and stable in a single mode optical fiber[5]. Thus, it was possible to use optical fibers as the beam path in an optical gyroscope. A ring interferometer was then built using 10 meters of fiber, and a similar experiment was performed using 950 meters[6] of single mode fiber. Next, a portable rotating Sagnac interferometer was constructed using 85 m of single mode fiber on a 20-inch diameter ring[7]. A fringe shift of 10^{-2} was measured which corresponded to about 2.1 degrees/sec (7600 degrees/hr). While the accuracy of this rotating Sagnac interferometer was not adequate for detailed evaluation as a gyroscope, it did indicate a

need for future studies in specific areas such as temperature effects, optical noise, mechanical noise, laser noise and electronics. In this report, although all these areas were studied, the fiber noise (optical noise) was the primary item of concern.

2.0 TECHNICAL DISCUSSION

2.1 Introduction

Experiemnts which demonstrated that fiber ring interferometers could be built have been completed[5][6]. The next research step in the study of the fiber gyroscopes is the investigation of noise sources.

It was apparent from previous research, for example, that motion of the interferometer components cause relatively large fringe (phase) shifts. Therefore, it was essential that the focusing lenses, beamsplitters, etc., be rigid or even replaced with equivalent fiber optical components. A fiber beamsplitter has been developed by NRL and NOSC. In addition, directional couplers are being developed by JPL for use in the fiber gyroscope. These, however, were not available for this research study.

Our research centered on the optical noise problems. We attempted to eliminate reflection by submerging the optics and detectors in an immersion fluid Some recent experiments (UURI and JPL) have shown that the polarization effects in the fiber (which cause fringe contrast fluctuations) can be eliminated by winding the fiber so that the coil remains in one plane. Therefore, one phase of our research was a study of polarization properties of fibers and fiber configurations.

2.2 Goal

The goal of this research was to evaluate experimentally the noise sources in a Fiber Ring Optical Gyroscope (FROG). There is interest in this type of research because of the potential advantages of an optical ring interferometer compared to conventional mechanical gyroscopes which are: 1) reduction of the instrument weight by at least an order of magnitude, 2) instant on

and off operation, 3) reduction of the instrument complexity, 4) cost reduction of the instrument, 5) no moving parts, thus higher reliability, 6) reduction of the required operating power, and 7) the potential of all solid state construction.

The UURI proposed to carry out the following tasks:

1. Design a laboratory breadboard experiment to determine the optical noise sources in the fiber ring optical gyroscope.
2. Fabricate the fiber ring optical gyroscope.
3. Investigate the optical effects which gave rise to instrument noise which will include, but not limited to the following:
   a) Polarization effects
   b) Intensity effects
   c) Reflection effects
4. Attempt to measure earth rotation.
5. Report the results.

2.3 Construction

The initial plan was to build a 20 cm diameter ring using 1 kilometer of optical fiber. It was, however, determined that a more useful system might be one with a 1 km diameter ring using approximately 1 mile (1.57 kilometers) of optical fiber. The coil and optics were to be mounted on a Genesco rate table and tilted at the local latitude as shown in Figure 1.

Because of the delay in obtaining the fiber, a fringe follower readout was first installed in the already existing fiber interferometer gyroscope (FIG) previously built for the NASA Office of University Affairs. An electronic system was built, such that the angular rate ω and angular position θ of the FIG were computed and displayed on LED's. Recall that the FIG was 50 cm in diameter and had 85 m of fiber on the ring. An accuracy of only ~10° in position

a

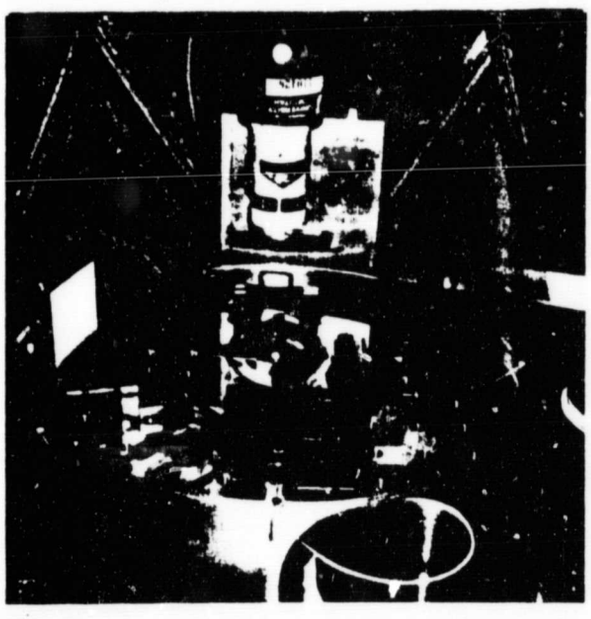

b

Figure 1. Fiber Ring Optical Gyroscope (FROG I). The top (a) shows the 1.57 kilometers of fiber mounted on the Genesco rate table. The bottom (b) shows the optics, fiber holders, and detector in the matching fluid.

(relative to a fiducial mark) was obtained. The fringe follower design was not pursued further. Figure 2 shows the FIG with the fringe follower and the LED readout.

To reduce the FROG optics to a small volume and eliminate one of the microscope objectives, 5 mm cube beamsplitters were mounted directly on a microscope objective. The microscope objective was sealed with a slipcover and the entire optical system including the detectors were immersed in a matching fluid to eliminate reflections. Figure 3 shows the container with the optical components immersed in fluid. The matching fluid had an index of refraction of 1,458 0.005 (n_c = 1.4557). The light from the laser was injected into the fluid through a partially submerged prism. Figure 4 shows various positions of the 1 mm diameter loop mounted on the Genesco rate table. The styrofoam was wrapped around the coil to promote thermal stability. The ITT optical fiber (as tested by the manufacturer) had 14.2 db/km attenuation at 6,300 Å. The attenuation at 8,800 Å was reported to be 3.11 db/km. The fiber was tested using an integrating sphere and a 3 mW laser source. An attenuation of approximately 8 db/km was obtained in the 1 m diameter coil configuration. In winding the fiber on the 1 m diameter loop, it was necessary to continually clean the fiber because of dirt on the outside covering. The winding device was constructed from a bicycle wheel to make the stringing of the fiber on the 1 m diameter ring more convenient. During the winding, the fiber was maintined under a tension of approximately 15 gmf. The fibers were wound side-by-side with about 60 turns across a 1-inch U-shaped based (see Figure 5). A sheet of mylar was placed between each layer until 8 layers were obtained with a total of 500 turns. Several bulges in the fiber were found. It appeared that blobs of material (looks like sawdust) were introduced during the teflon coating process. Subsequent discussions with ITT revealed that the teflon base which comes in the form of

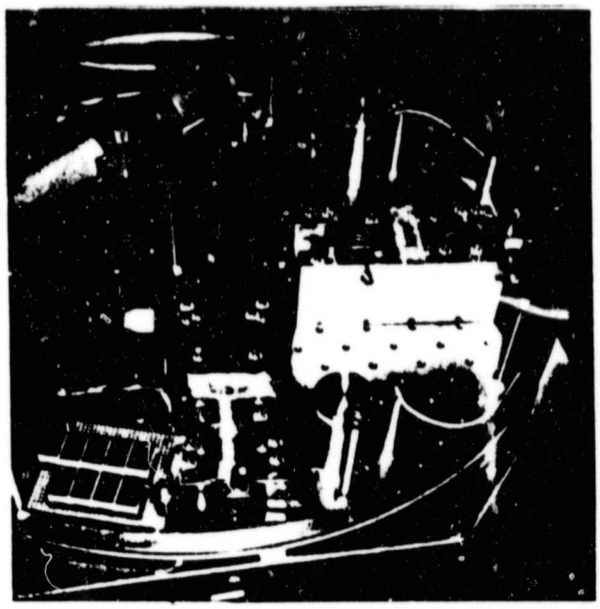

Figure 2. Fiber Interferometer Gyroscope (FIG) showing the fringe follower, LED read-out of position, and angular rate.

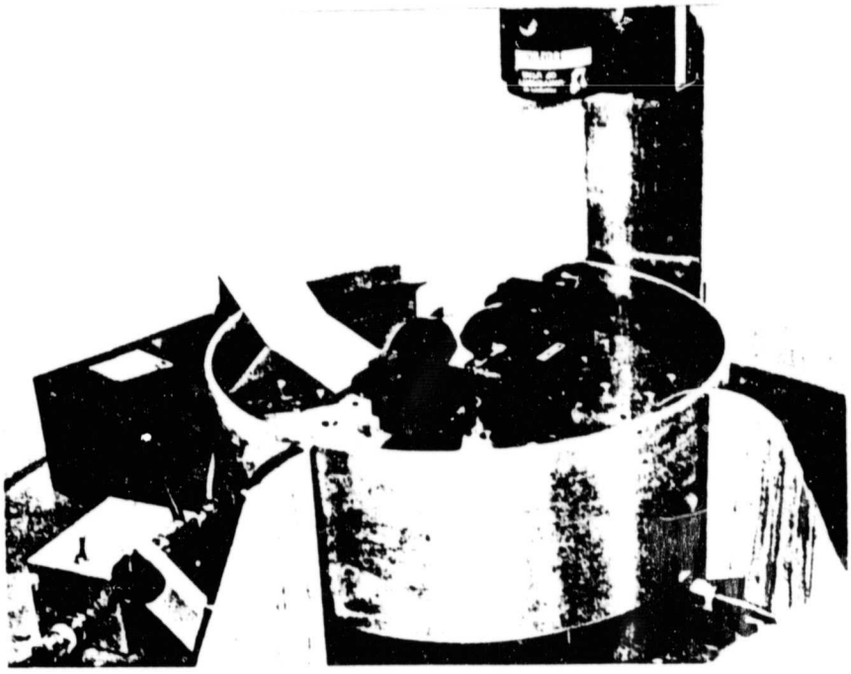

Figure 3. Top view of FROG I with matching fluid. The 8 meters of fiber are taped to the surface of the table to allow preliminary alignment.

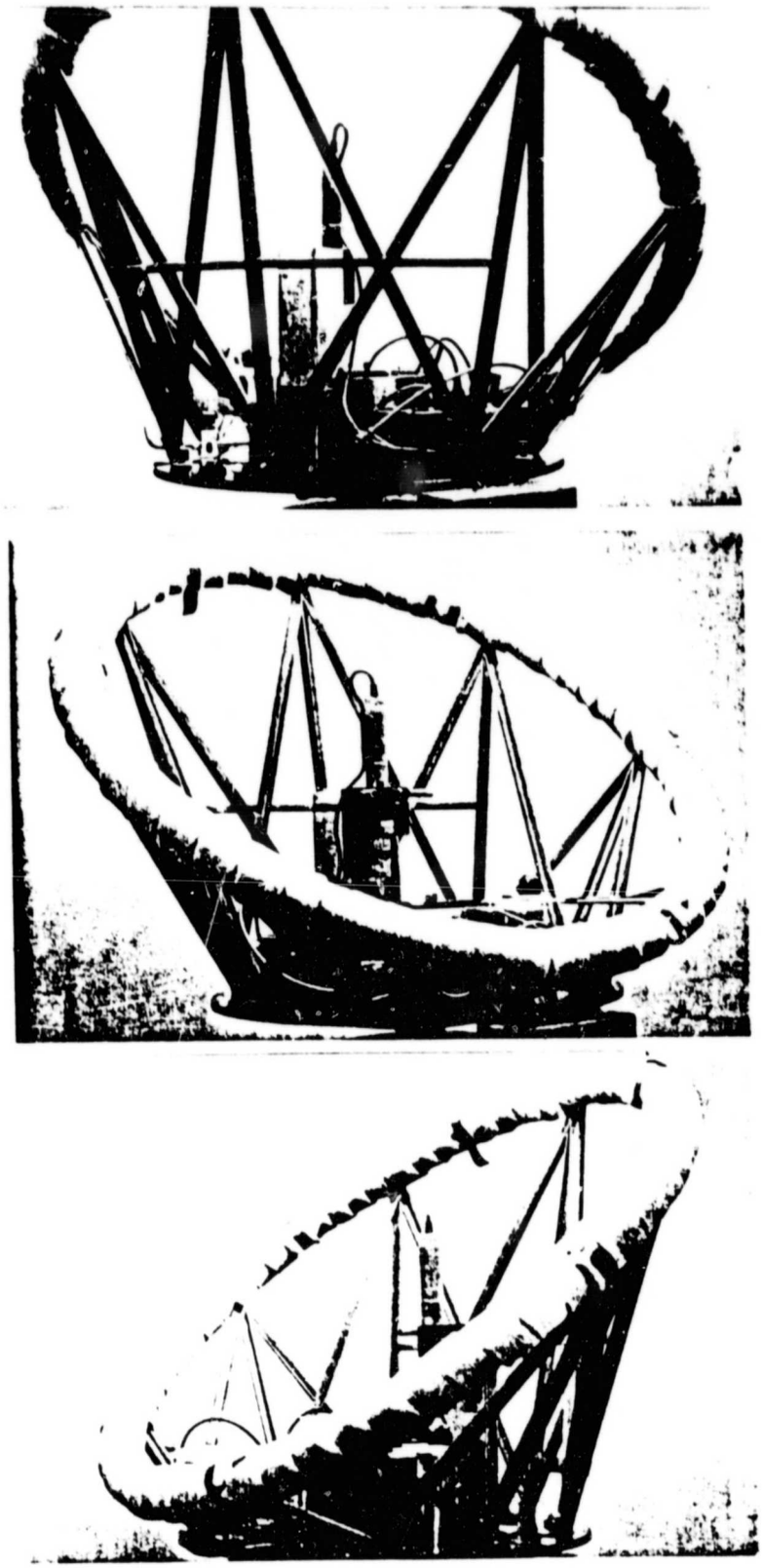

Figure 4. Various positions of the FROG I. In this version, the detector/amplifier was outside the fluid. The styrofoam was wrapped around the coil to promote thermal stability.

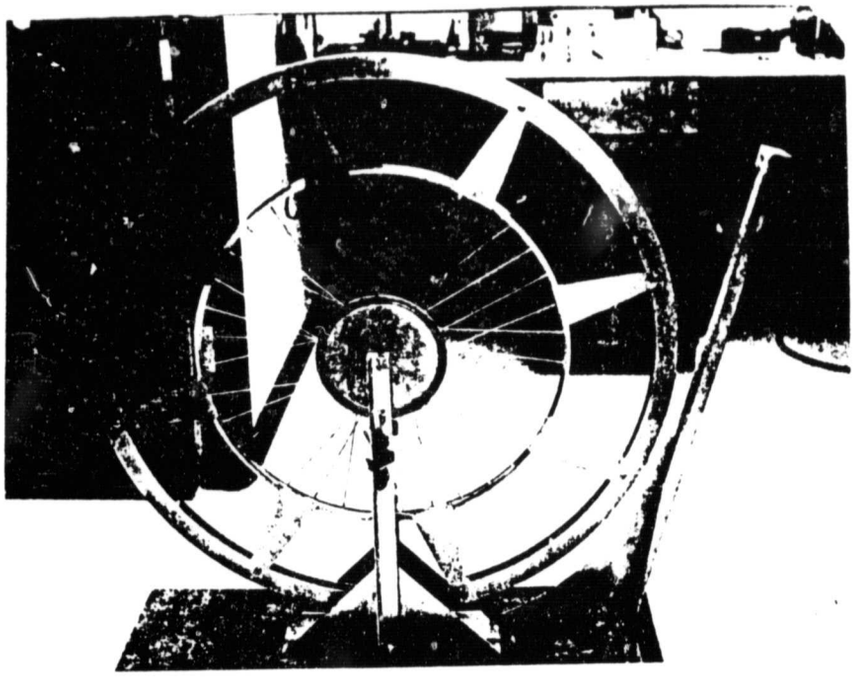

a

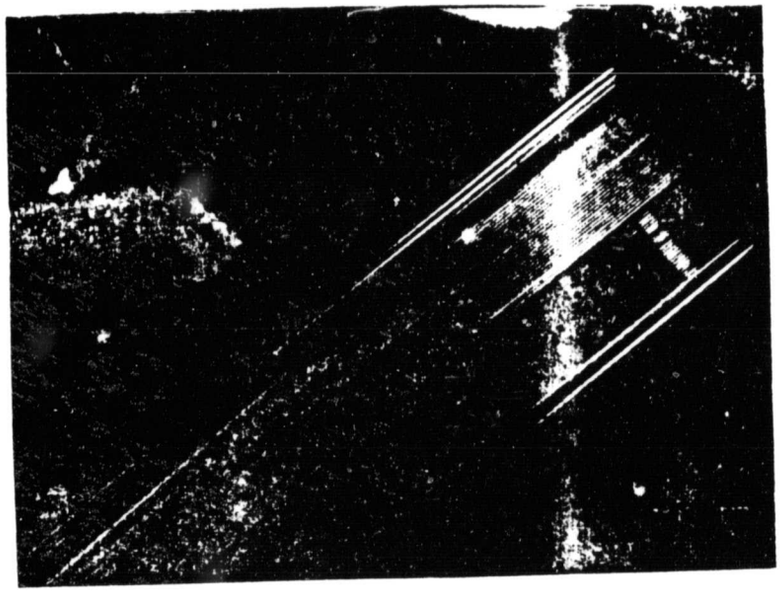

b

Figure 5. Winding mechanism was a bicycle wheel with the 1 meter ring mounted on the periphery (a). The coil was wound with the fiber side by side (b).

pellets may have aged. This does not affect the performance of the fiber. It would be useful in the future to request only new material be used. To accomodate these bulges, small holes were cut in the mylar sheet to minimize the effect on subsequent layers. Another problem found during the winding of the coil was that the fiber was twisted on the original drum. It was necessary to manually rotate the supply drum to take the twist out of the fiber. The gyro had the following parameters: The coil was mounted at 40.74° (the latitude of Salt Lake City, Utah), the average loop diameter was 100 ± 0.05 cm. The measured deviation from a circle of the coil was less than 0.1 cm. The coil consisted of 500 turns plus 0.3 of a turn due to the connecting optical components; therefore, the total length of the fiber was estimated to be L = 1571.7 ± 0.3 meters. The fiber core diameter was about 5.5 micrometers.

Preliminary testing (Section 2.4) indicated that immersion in matching fluid of the interferometer parts including the fiber ends appeared to be successful in eliminating unwanted fringe patterns. The plan was then to rotate the coil very slowly which modulated the fringe shift and thus, which would detect the earth rotation. If the system turned out to be too noisy, it was planned to advance the coil several degrees at a time and leave stationary while measurements were made. Figure 6 shows the geometry of the mounting, The modulation expected was,

$$\Delta Z = \frac{2\omega LR}{\lambda c} \quad ,$$

$$\Delta Z_E = \frac{2 \cdot 7.27 \cdot 10^{-5} \cdot 1.57 \cdot 10^{5} \cdot 50}{6.33\ 10^{-5} \cdot 3.10^{10}}$$

$\Delta Z_E = 6.01 \times 10^{-4}$ fringe shift due to Earth rate.

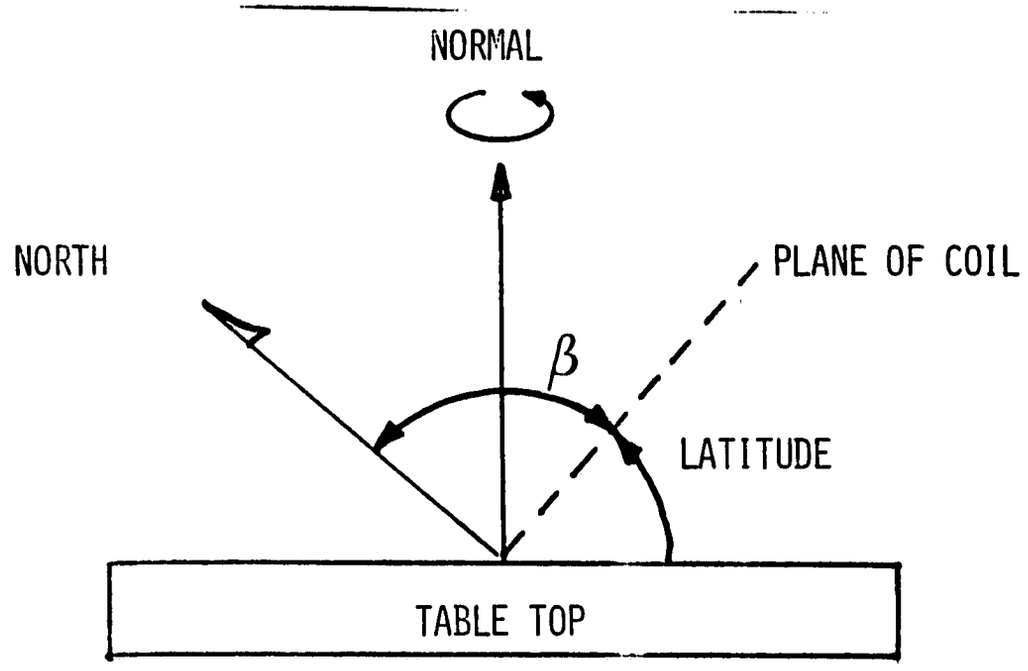

$\leq \beta \leq 81.^{\circ}48$

LATITUDE (SLC) = $40.^{\circ}74$

Figure 6. The geometry of the mounting used in the attempt to detect earth rotation rate.

The modulation predicted would be

$$\Delta Z_E \sin 81°49 = 0.989\ \Delta Z_E \quad .$$

In July of 1978, a performance review was held at the Jet Propulsion Laboratory. As a result of this performance review, a new test plan was developed which included rework of: the electronics, preamplifier, amplifier, ratio circuit, etc. The new plan was to: measure the noise level, evaluate the ratio circuit, incorporate a synchronous detection system, test optical isolators, test for stress-induced birefringence and polarization effects, observe and record thermal effects, and observe and record mechanical effects. The results of these tests will be discussed in Section 3.0 Evaluation.

On May 3, 1978, Dr. Vali left the Geospace Sciences Laboratory of the University of Utah Research Institute. At that time, Dr. Glen J. Morris was appointed Principal Investigator and continued so to the end of the project. On July 5, 1978, Dr. Lawrence D. Weaver joined the Geospace Sciences Laboratory and was responsible for carrying out the remaining portion of the research.

2.4 Preliminary Testing

The FIG (Fiber Interferometer Gyroscope) with an electro-mechanical fringe follower (visa-corder mirror galvo) was tested and found to have a pointing accuracy of only ±10°. The test of this system was discontinued because of the poor results. Mechanical instability was assumed to be the primary cause of the difficulty.

The optical system of the FROG (Fiber Ring Optical Gyroscope) was immersed in a matching fluid to reduce the fiber end reflections. Figure 7 shows the method used. A small loop of fiber (8 meters) was taped to the surface of the table (see Figure 3). A substantial reduction in the end reflections was observed visually.

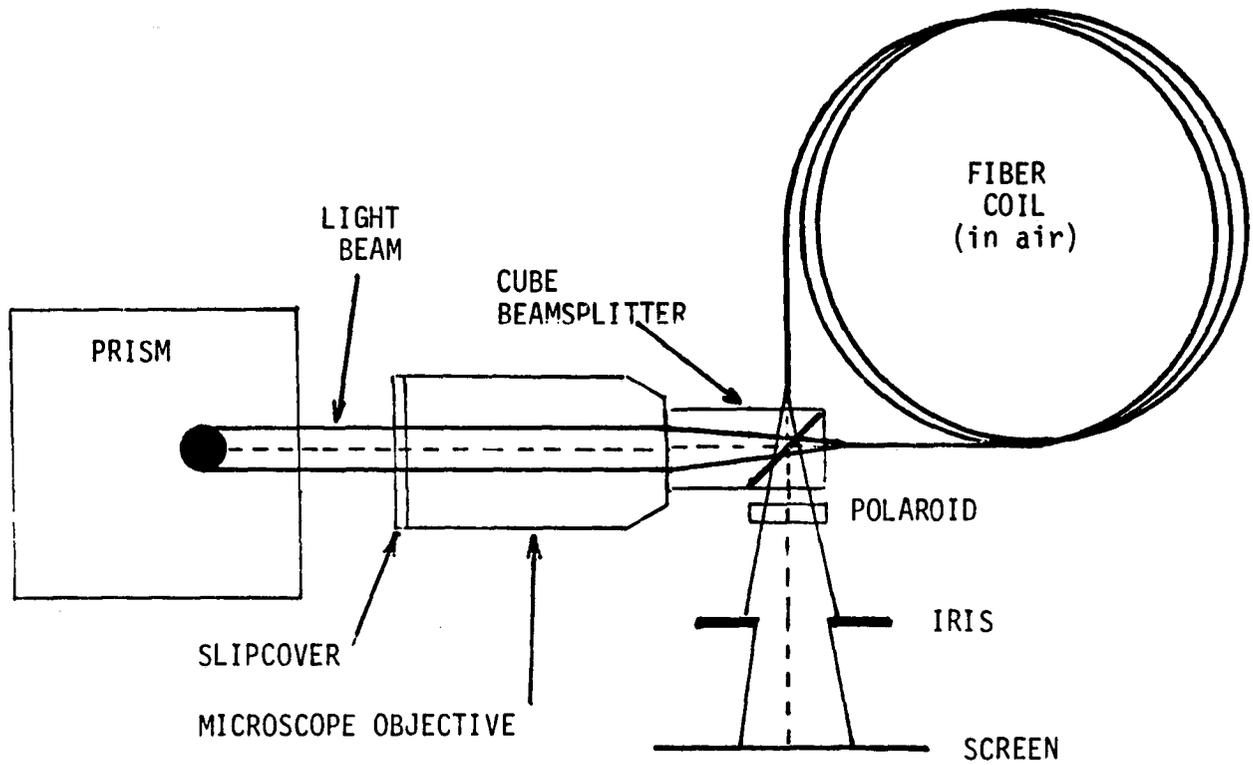

TOP VIEW

Figure 7. Diagram of FROG I optics immersed in matching fluid. See Figure 8 for detail of PRISM.

A second system was constructed using another 5 mm cube beamsplitter to observe the complementary fringe pattern. Figure 8 illustrates the arrangement. Reflections, however, from the surface of the liquid made it inconvenient to use detector #1. In the final configuration, only detector #2 was used to measure fringe shift as shown in various views in Figure 9.

The configuration used in the attempt to detect earth rotation was shown in Figure 4. The results of this test by Vali and Berg are given in Appendix A. Their results were interpreted in terms of nonreciprocity noise in the fiber gyroscope. There is no evidence that the earth rotation rate was detected.

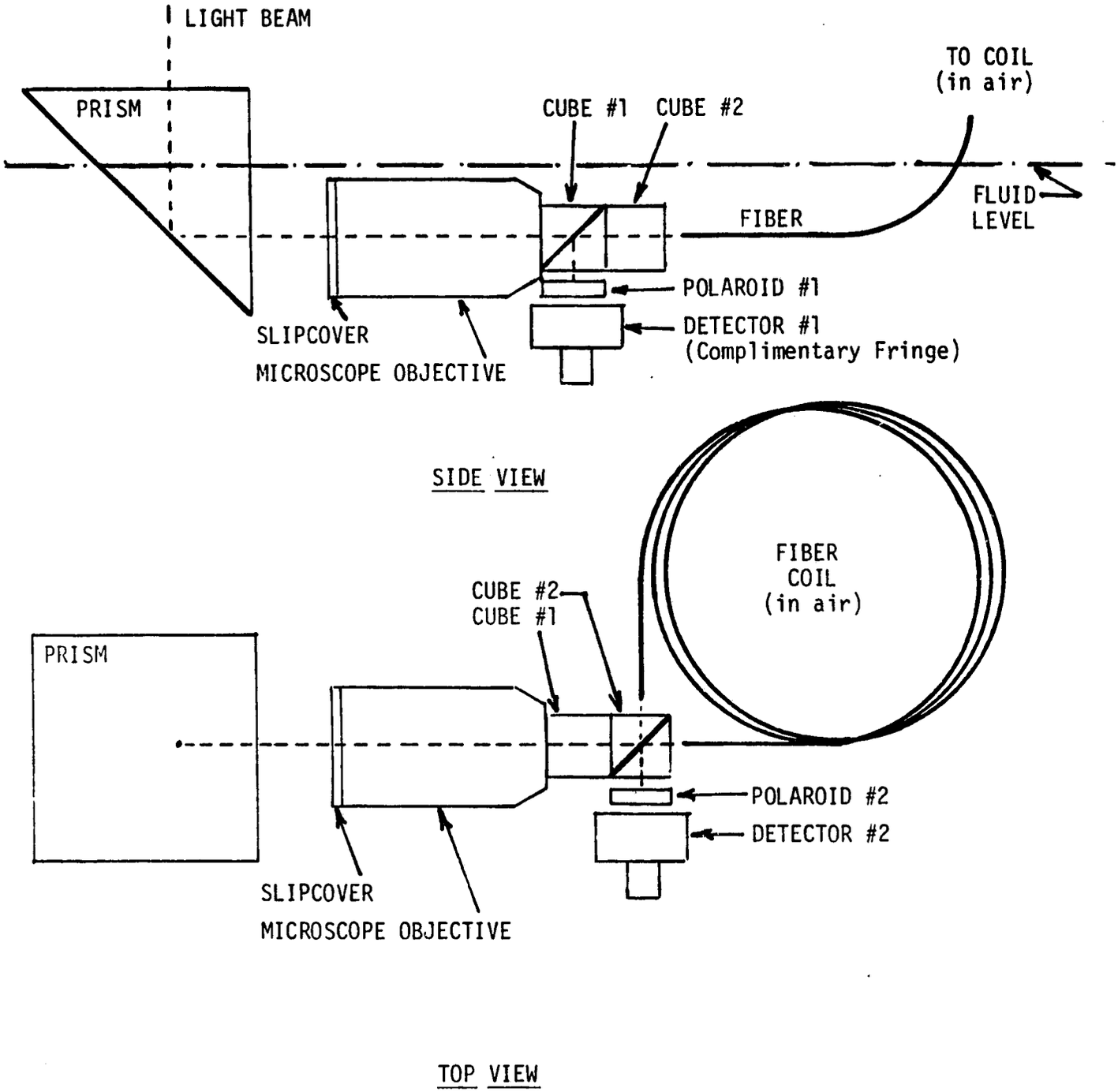

Figure 8. Diagram of second design of FROG I to observe complimentary fringe.

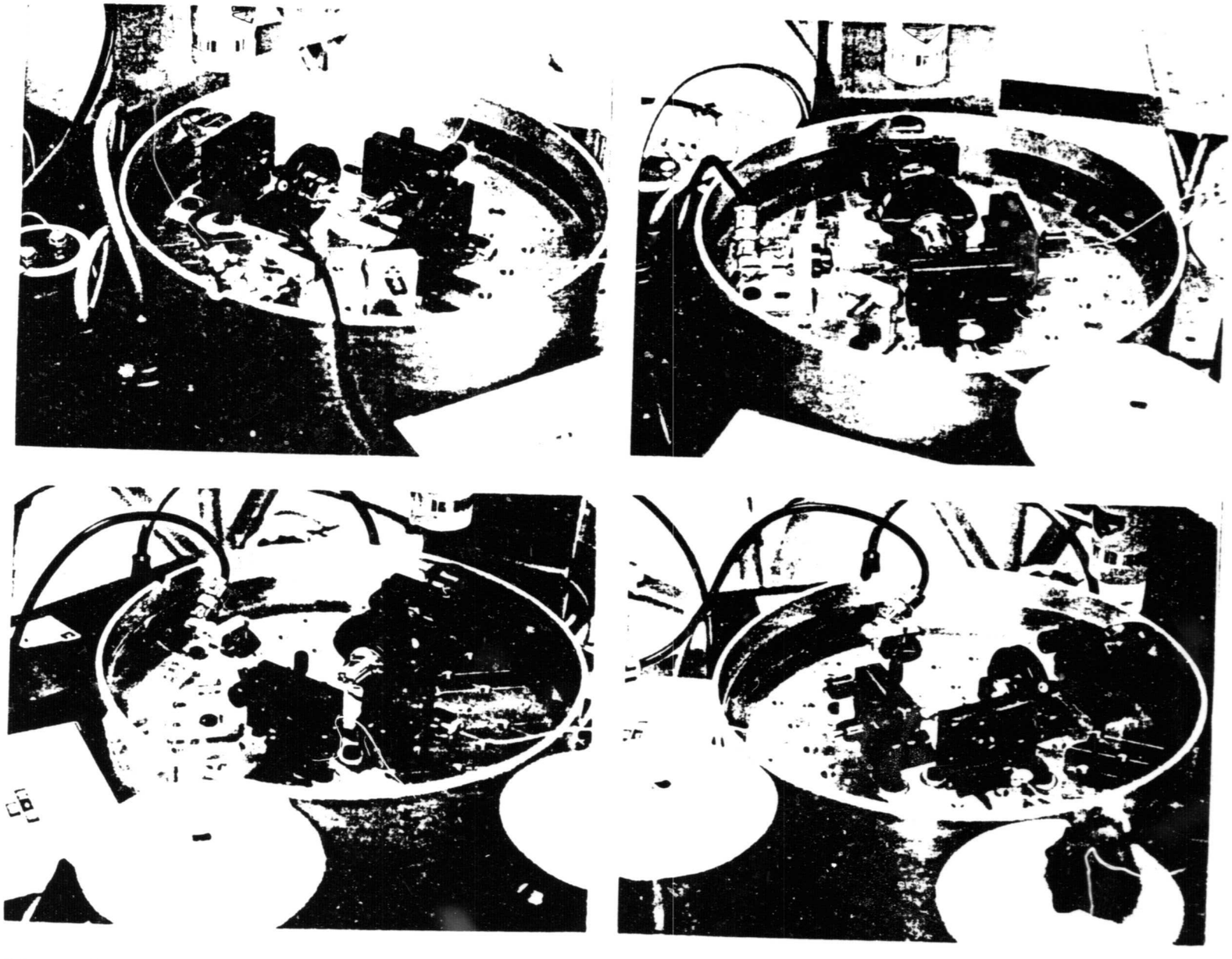

Figure 9. Various views of the immersed optics. Only one detector was used in the measurements.

3.0 EVALUATION

As originally conceived, the FROG I was to utilize a DC detection method for the measurement of fringe intensity. After the results of the preliminary testing, a synchronous detection scheme was added. The dominant sources of noise that were present in the FROG I were attributed to: source laser intensity fluctations, electronic noise, opto-mechanical noise, and stray reflections. Each of these were separately evaluated in order to ascertain their relative contribution to the total noise.

3.1 Characterization of the FROG I Detection System

The block diagram of the electronics system used in FROG I is shown in Figure 10. In this method, fluctuations in the laser intensity were to be handled by splitting off a portion of the He-Ne beam before allowing it to enter the fiber ends, measuring the beam intensity, and forming the ratio of the output fringe intensity to the reference beam intensity. This method does not, however, take into account changes in fringe intensity that are brought about by changes in the coupling efficiency of the beam into the fiber. These changes in the coupling efficiency were a major source of drift and noise in the FROG I. A better approach would have been to use a second fringe detector (looking at the complimentary fringe pattern), form the difference and sum signals, and take the ratio between the two. Unfortunately, the FROG I was designed in such a way that the complimentary fringe pattern was not readily obtainable.

Each component illustrated was a source of noise and consequently was characterized. For example, the output of the fringe detector preamp was typically 300 mv at $\omega = 0$. The detector/preamp combination (Silicon Detector Corporation

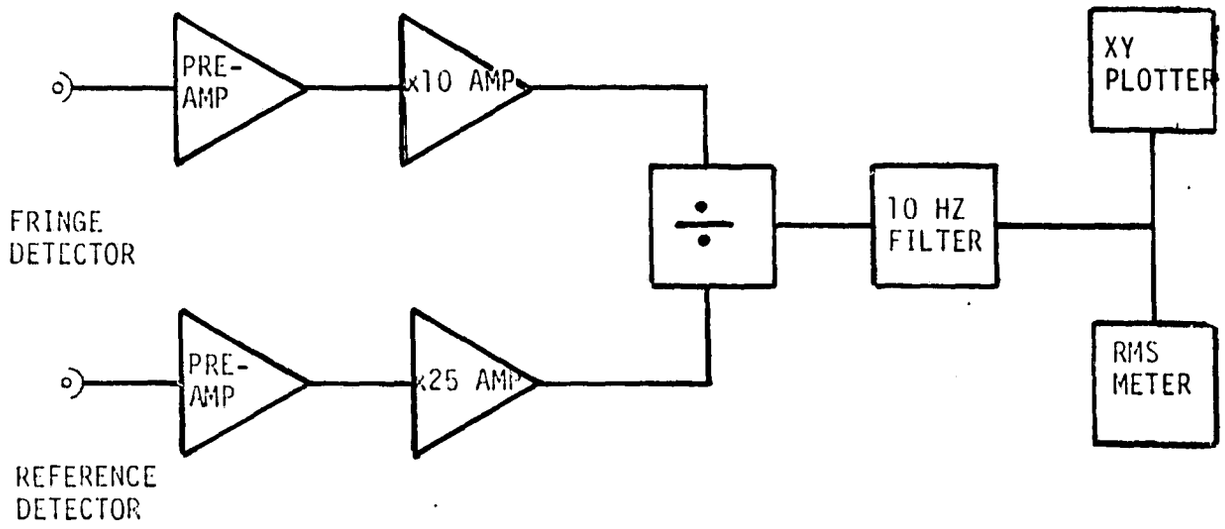

Figure 10. Block diagram of the electronic system used in FROG I.

SD-100-42-12-231) had a rms noise output of 230 μv. Although the preamplifier had only a 100 Hz 3 db signal bandwidth with respect to incoming light, the noise bandwidth (at the output of the preamp) was somewhat greater (the 10 Hz low pass filter was not available for these measurements). Thus, the fringe detector preamp had a signal-to-noise ratio

$$S/N = \frac{.3v}{.23 \times 10^{-3}v} = 1300. \qquad \text{(D.C. signal/AC RMS noise)}$$

The x 10 amplifier in the fringe detector circuit had an output noise level of about 60 μv(again, wideband). Since 10 x 230 μv = 2300 μv >> 60 μv, the detector or/preamp combination was the major source of electronic noise for the measurements described in Appendices A. Similar considerations for the reference detector (laser intensity monitor), but with different noise and signal levels, indicated a signal-to-noise ratio of S/N = 1750.

The divider, or ratiometer (Analog Devices Model 436A), was another source of instrumentation noise. This device was extensively characterized over a wide range of input levels and modulation depths. Since the output of the laser was constant to within ±(0.5 - 1.0)% on a RMS basis and with peak excursions to ±2%, the output noise level measured in a simulated experiment indicated a S/N = 4300. In that measurement, the denominator input was 10v ± 1.5% and the numerator was at midrange (~3v) corresponding to a fringe detector output biased to a 90° phase shift. Again, the S/N quoted is a wideband figure.

For the experiments whose descriptions follow in the next section, the bandwidth of the electronics was restricted to about 10 Hz. Thus, the signal-to-noise ratios were greatly improved. The actual S/N (of the electronics) for these experiments were not measured since the results indicated a much lower value than would be anticipated even with the wideband S/N ratios.

3.2 Performance of FROG I - DC Detection System

In order to assess the performance of the FROG I, the output of the fringe detector was monitored for several minutes at each data point thereby obtaining drift and noise data. The 10 Hz bandwidth of the electronics should have provided an adequate S/N ratio (S/N >> 1300) for detecting Earth rotation (provided the interferometer is biased to approximately 90°). In the experiments that were conducted (see Appendices A), the outputs of the fringe and reference detectors were not ratioed. In view of the results obtained, this step was not required.

Figures 11 and 12 are x-y plots of the fringe and reference detector outputs with no rotation. During the course of these measurements, it was observed that spurious signals were being generated by the interference between beams that were (most likely) derived from reflections with the cube beamsplitter or else from the fiber ends, recalling that all of the optics were immersed in index-matching fluid to eliminate these reflections. However, the index of refraction was only matched to the fiber to reduce end reflections and not reflections from other components. These effects (fringes caused by reflections) could be reduced by upconversion to a frequency (via an audio speaker attached to the rate table) outside the bandwidth of the electronics (refer to Figures 11 & 12). However, for rotation rates > 0, this technique did not result in any improvement in the noise level (Figures 13 & 14) because of the vibration introduced by the table during rotation. The residual higher frequency components observed in Figure 10 could be reduced by allowing the matching fluid to settle overnight (Figure 15). The upper trace in Figure 15 is the one obtained after the system was allowed to settle overnight, and the lower trace was obtained after a minor perturbation of the fluid. Figure 16 shows the traces obtained after highly perturbing the fluid. These measurements (Figures 15 & 16) were obtained with

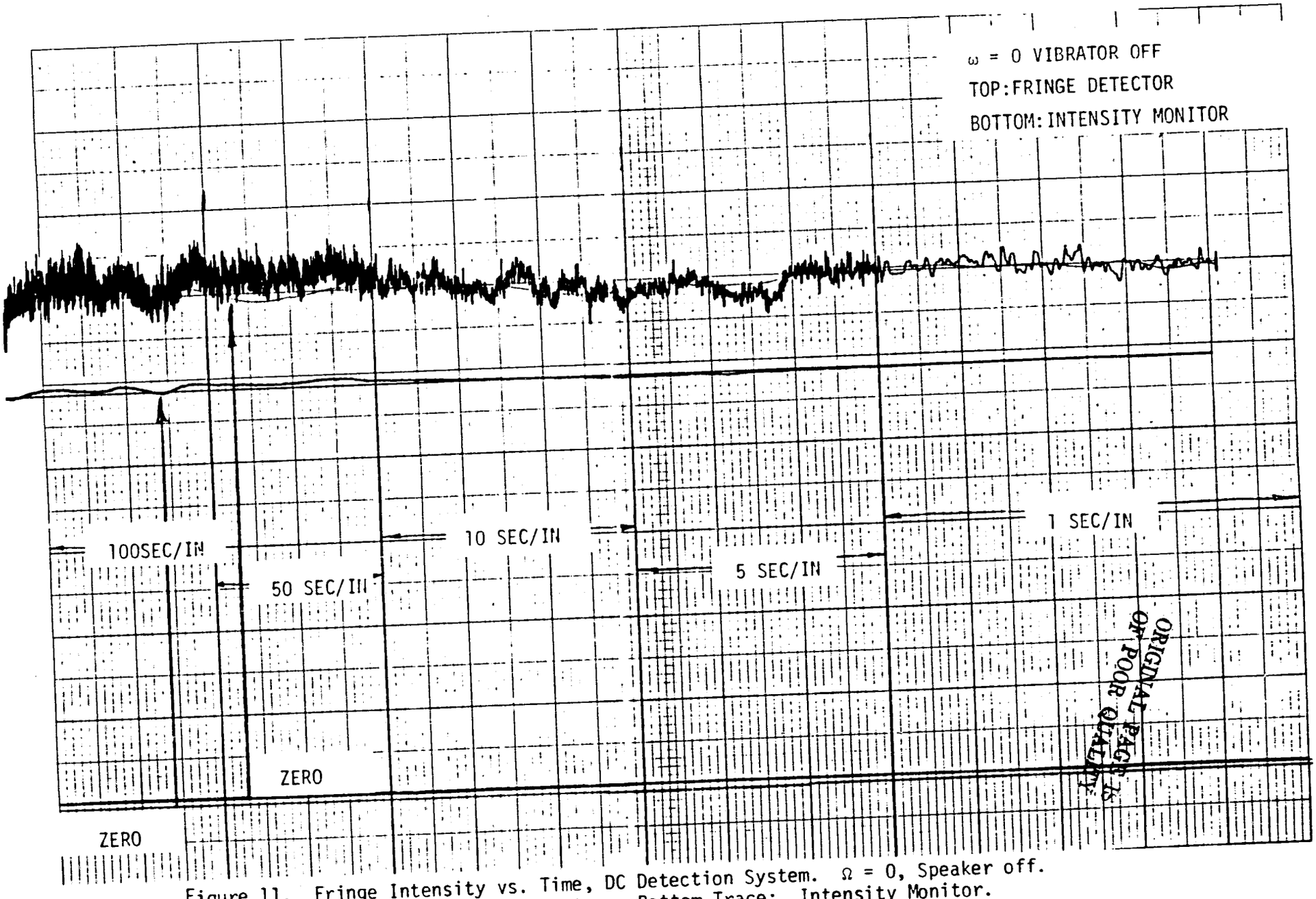

Figure 11. Fringe Intensity vs. Time, DC Detection System. Ω = 0, Speaker off. Top Trace: Fringe Detector. Bottom Trace: Intensity Monitor.

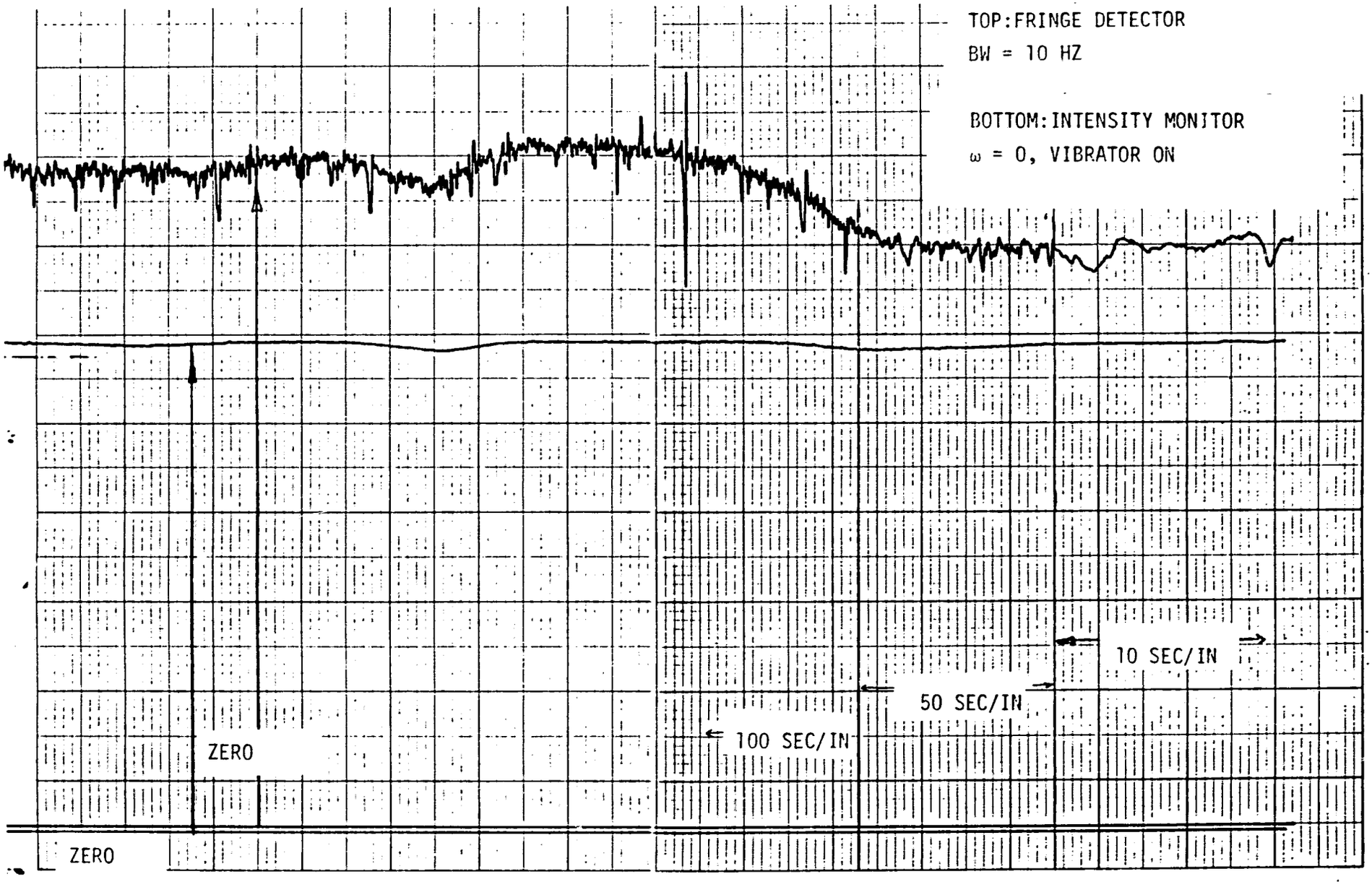

Figure 12. Fringe Intensity vs. Time, DC Detection System. $\Omega = 0$, Speaker on. Top Trace: Fringe Detector. Bottom Trace: Intensity Monitor.

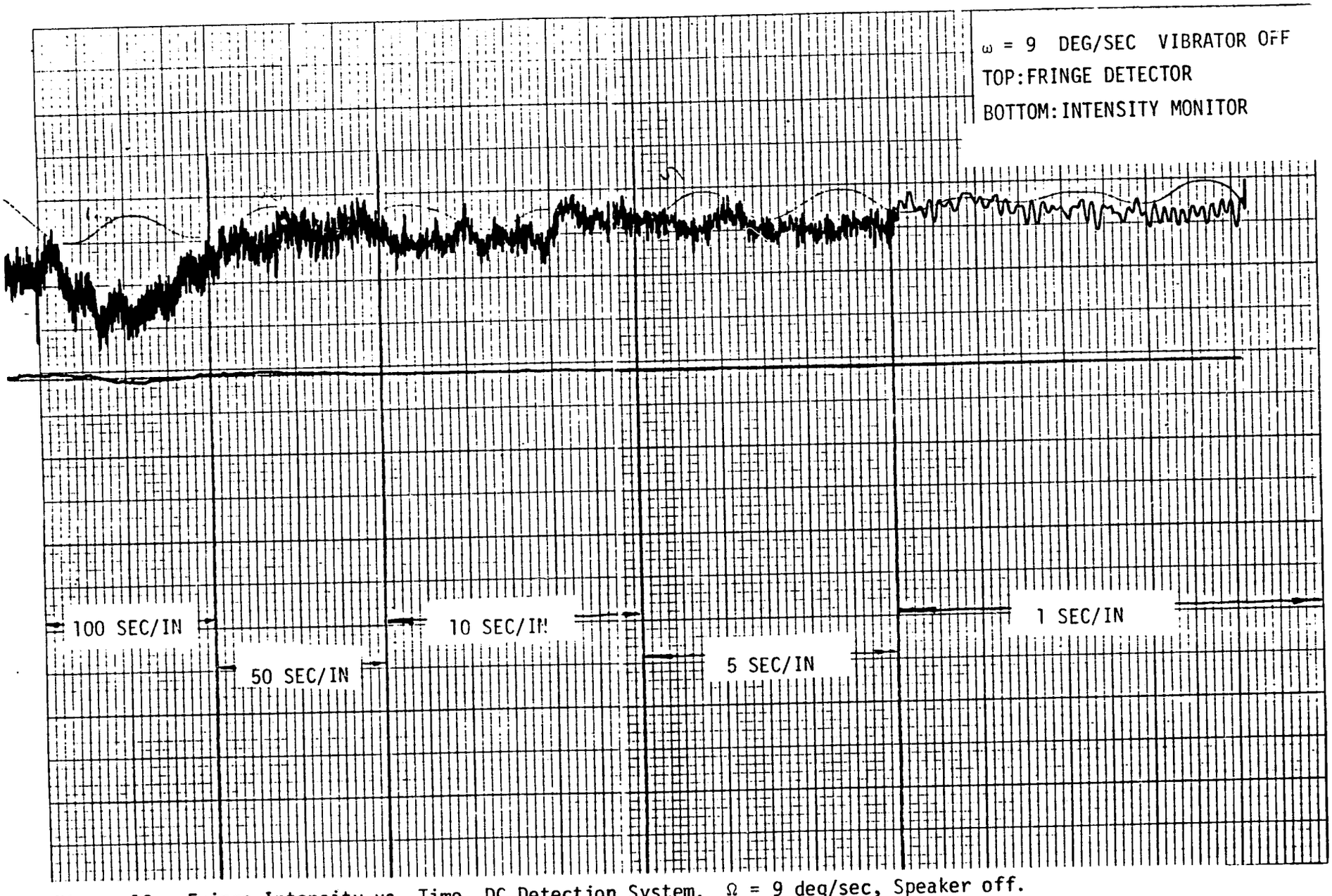

Figure 13. Fringe Intensity vs. Time, DC Detection System. Ω = 9 deg/sec, Speaker off. Top Trace: Fringe Detector. Bottom Trace: Intensity Monitor.

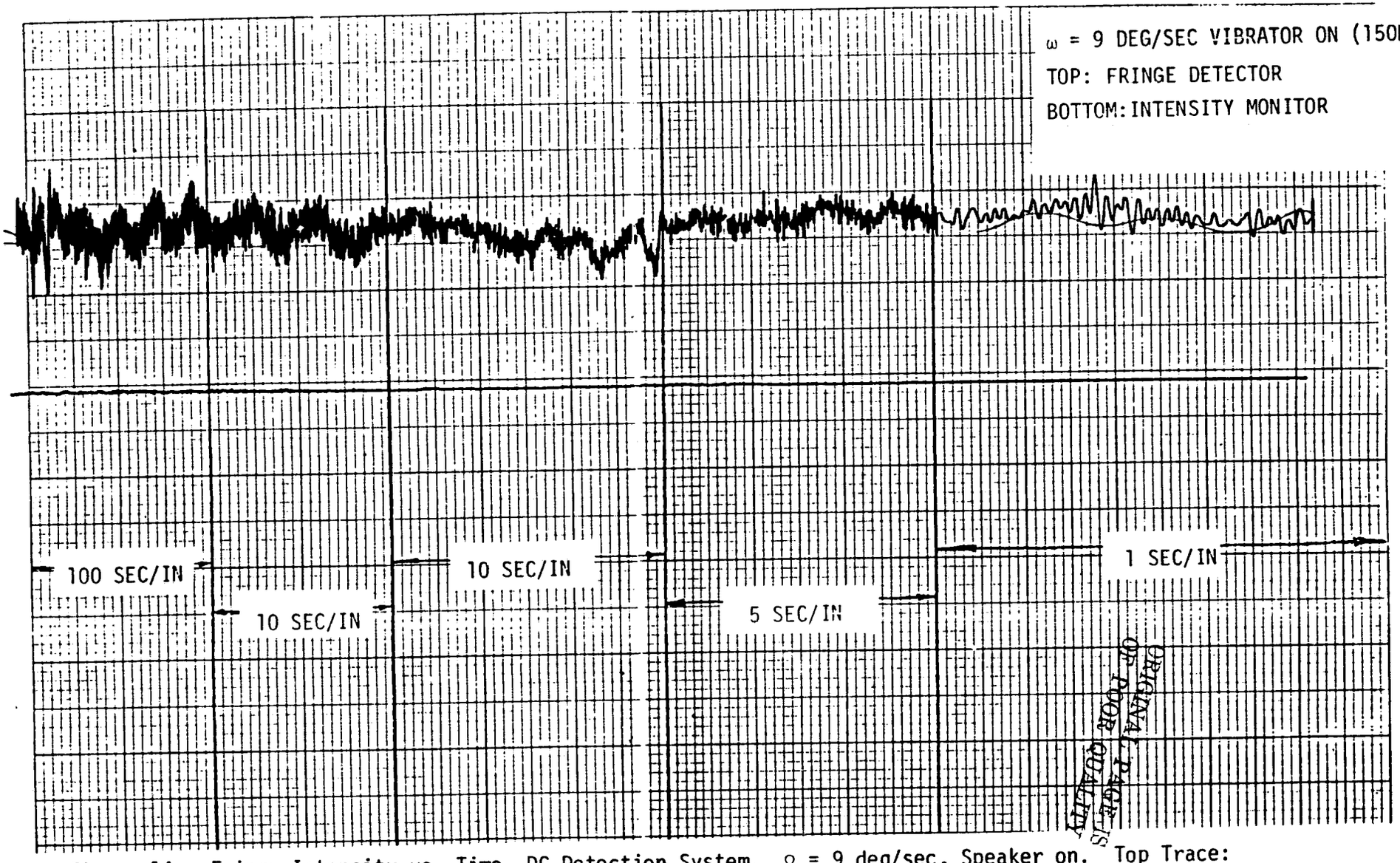

Figure 14. Fringe Intensity vs. Time, DC Detection System. Ω = 9 deg/sec, Speaker on. Top Trace: Fringe Detector. Bottom Trace: Intensity Monitor.

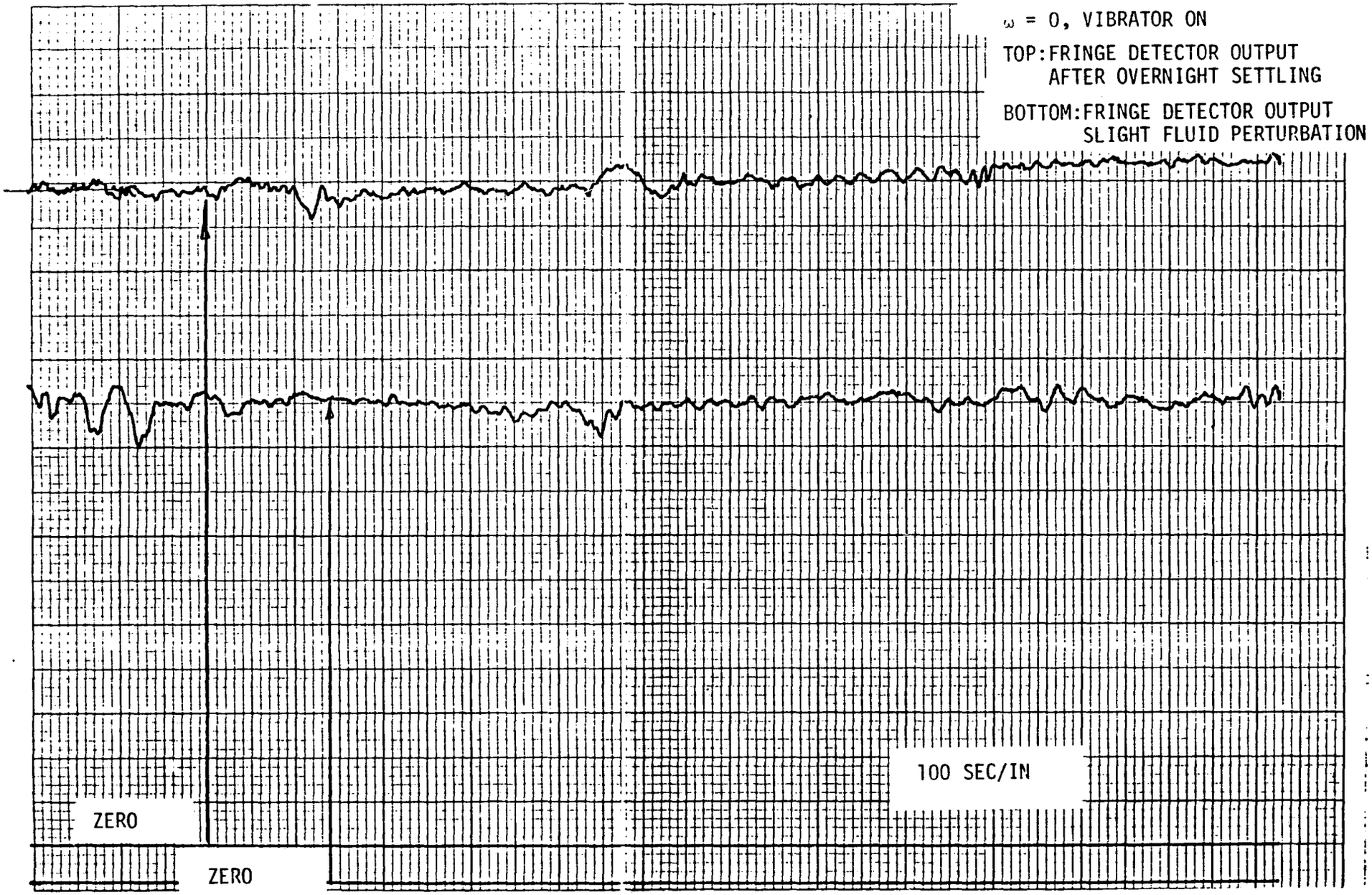

Figure 15. Fringe Intensity vs. Time, DC Detection System. Ω = 0, Speaker on. Top Trace: Fringe Detector output after overnight settling. Bottom Trace: Fringe Detector output with slight fluid perturbation.

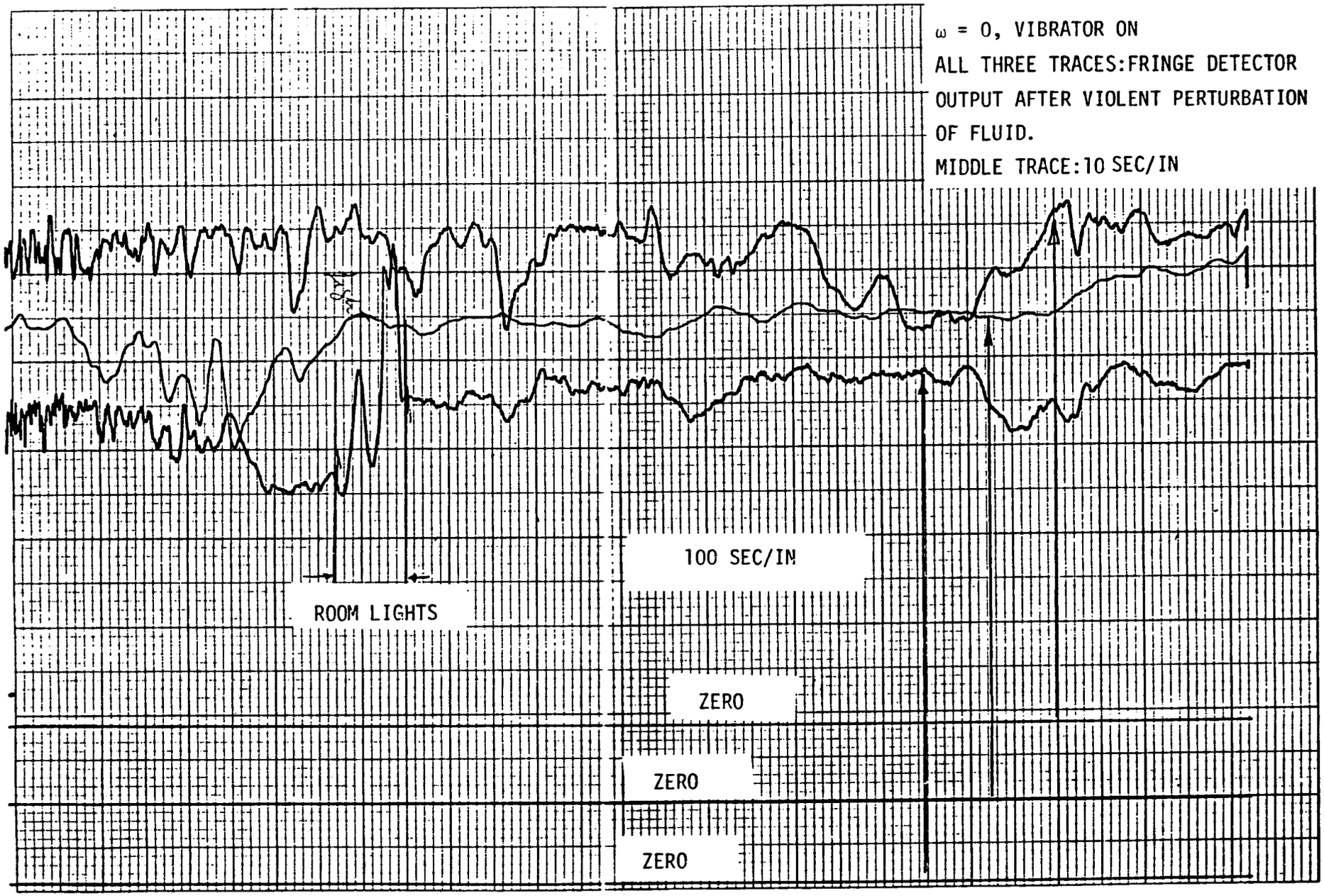

Figure 16. Fringe Intensity vs. Time, DC Detection System. Ω = 0, Speaker on. All traces: Fringe Detector output after violent perturbation of fluid. Middle Trace: 10 in/sec.

the speaker on, thus reducing the noise components associated with stray reflections.

Thus, it must be concluded from these measurements that another source of "noise" is that due to the fluid. More precisely, the source is due to particles suspended in the fluid which in turn produce scattered and diffracted components in the beam. Even in the absence of external perturbations, Brownian motion of the particles therefore is capable of inducing temporal changes in the received flux (i.e., "noise").

Although the fluid was quite "dirty" after several months of use and undoubtedly was a source of ever-increasing noise, its utility as an inhibitor of end reflections is open to question, particularly since it does not eliminate stray reflections from other optical components. Of greater concern were the slow temporal variations present in Figures 11-16. These are discussed in the next section.

3.3 Performance of FROG II - Synchronous Detection Method

A serious problem with DC detection methods is the offset drift always present in DC amplifiers. Offset drift errors in the preamplifiers and amplifiers used in the FROG I amount to a few millivolts (over periods of 30 minutes to an hour or more) and are especially large when referred to the fringe detector preamp output. In that case, the error due to drift is somewhat larger than the S/N ratio indicates.

One means of circumventing the electronic drift problem is to convert the optical signal to an AC signal and use synchronous detection methods. There are, in general, other advantages to this technique, but these shall not be discussed here.

In the method used for FROG II, the laser beam entering the fiber ring interferometer was mechanically chopped at ~1600 Hz (see Figure 17). The beam impinging on the reference detector was unchopped due to lack of a 2nd channel in the lock-in amplifier. The output of the fringe detector was synchronously detected by an Ithaco Dynatrac Lock-In Amplifier.

Figure 18 illustrates typical outputs from the fringe and reference detectors. The bandwidth of the lock-in is 0.03 Hz and the output time constant was 4 sec. The high noise level could be due to: (1) Intensity fluctuations produced by particles in the fluid. (2) Noise generation due to polarization fluctuations produced in the fiber by changes in the birefringent properties of the fiber. (3) Changes in the optical coupling efficiency into the fiber.

In Figure 19, the bandwidth was reduced to 0.001 Hz with a corresponding increase in the output time constant to 125 seconds. It is seen here when the noise component has been smoothed, that there are long-term drifts in the output of the fringe detector which are not correlated with changes in the laser output. The most probable cause for this effect are changes in the coupling of the beams into the two fiber ends. The five-axis fiber positioners used were not stable alignment devices. In addition to vibration, which can be readily transmitted to these positioners, they also possess a slow hystersis which is responsible for long-term drift in the fringe detector output.

Incorporation of a synchronous detection system into the FROG II cannot solve these drift problems since any real changes in the received optical power (due to either laser intensity changes or changes in the coupling efficiency) are synchronous at the chopping frequency (i.e., they are correlated with respect to the signal). Noise components that are uncorrelated with respect to the signal are the only one rejected.

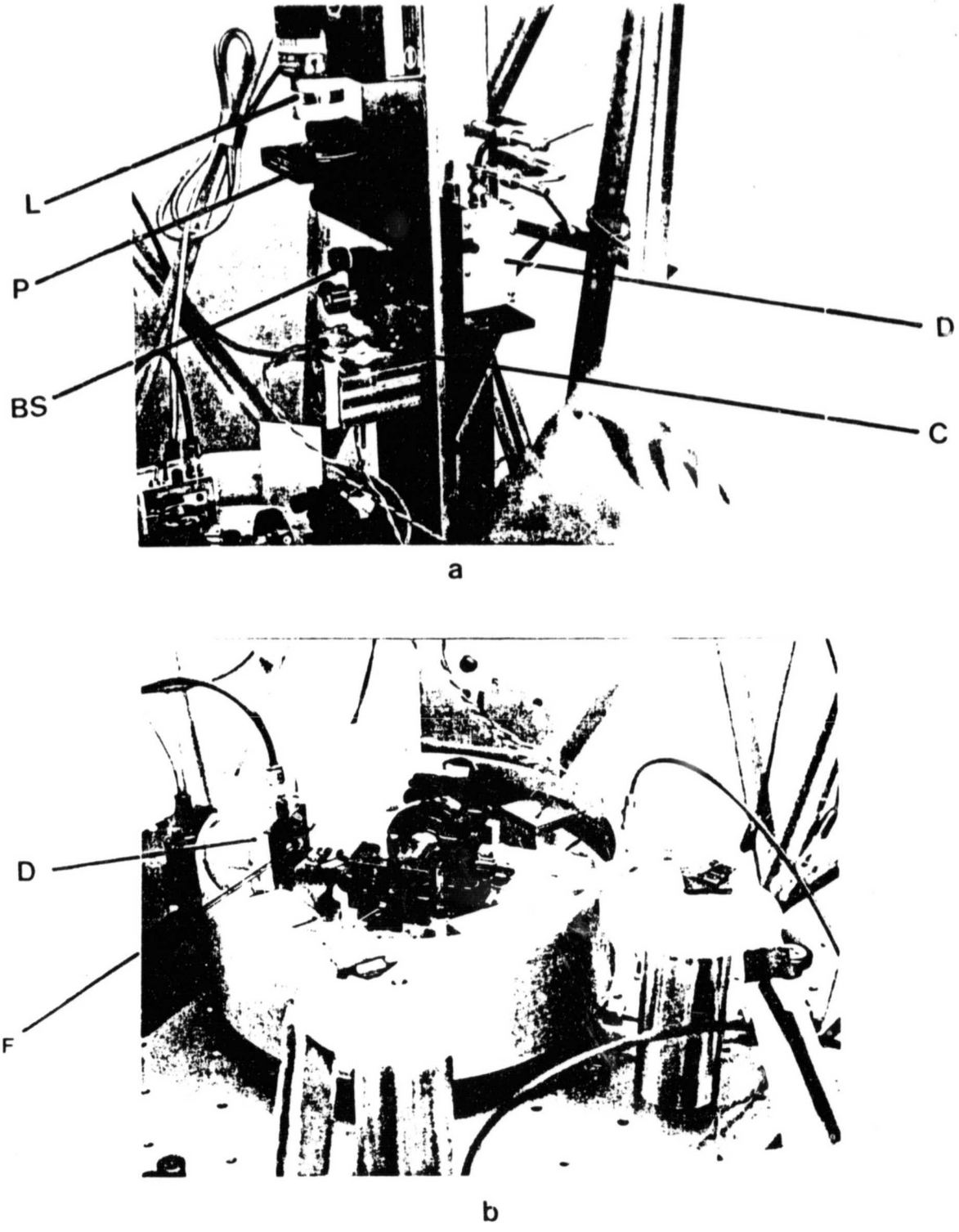

Figure 17. Photograph of FROG II. In the top photo (a), the laser L, polarizer P, beamsplitter BS, laser reference intensity monitor detector/amplifier D, chopper C, are shown. In the lower photo (b), the detector/amplifier for observing the fringe pattern F are shown.

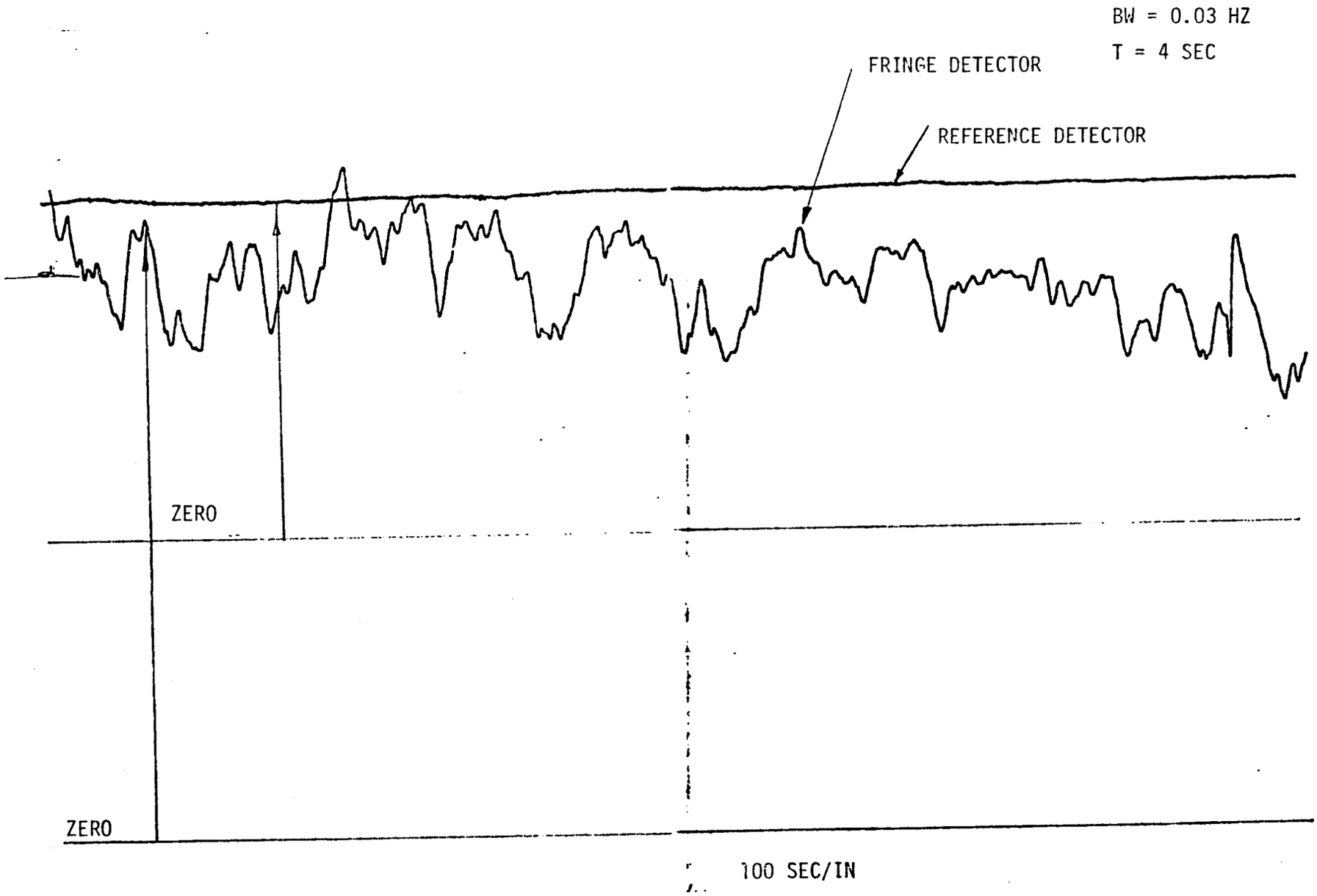

Figure 18. Fringe Intensity vs. Time, Synchronous Detection System. Ω = 0, Speaker on. BW = 003 Hz, Time constant = 4 sec.

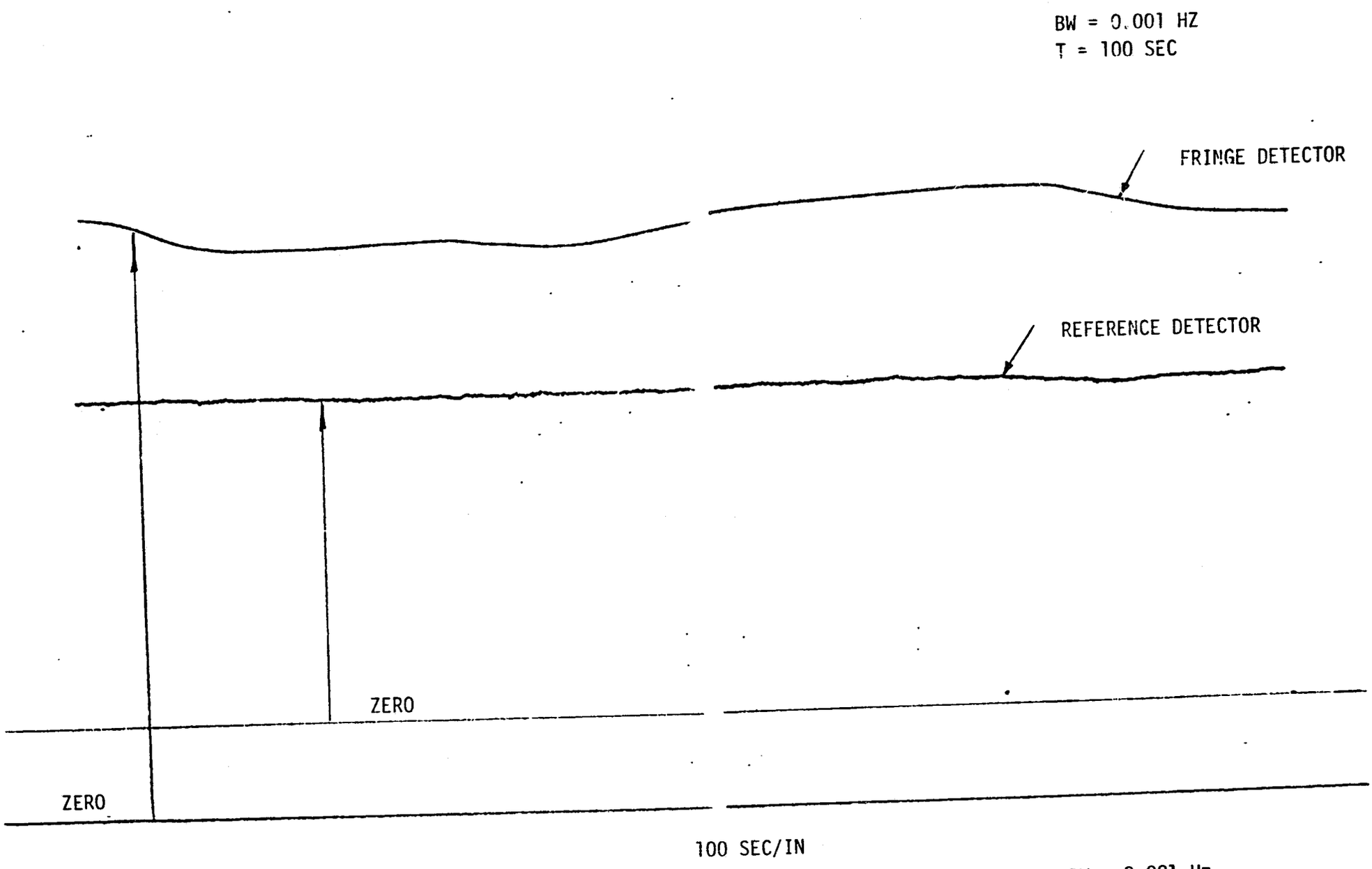

Figure 19. Fringe Intensity vs. Time, Synchronous Detection System. Ω = 0, Speaker on. BW = 0.001 Hz, Time constant = 100 sec.

3.4 Source Isolation

Feedback of energy into the Helium-Neon laser source was not a problem with the FROG II since other sources of noise and drift dominated the measurements. However, one method of isolating the source from feedback was investigated. This involved the use of quarter-waveplate optical isolators. These were found to be somewhat effective in reducing the laser intensity fluctuations as monitored with the reference intensity detector. In general, they may not be useful in a fiber interferometer since their effectiveness is determined by the polarization state of the returned beam.

A better method for eliminating the feedback, as well as reducing the interference effects from stray reflections, is to pulse the laser source on and off at a rate determined by the propagation time in the fiber.

3.5 Polarization Measurements

A fiber interferometer is an example of a class of interferometers known as common path interferometers. In this type of interferometer, both beams traverse, in opposite directions, the same geometrical, if not the same optical, path. Consequently, this class of interferometers is relatively immune from the effects of vibration and reciprocal path length changes. A single mode optical fiber, so named because only one transverse mode of propagation can because only on transverse mode of propagation can be supported, is actually capable of propagating two orthogonal modes of polarization. Single mode optical fibers are known to exhibit linear birefringence and perhaps circular birefringence (optical activity). Some researchers have expressed concern that the polarization cannot be preserved in a fiber due to stress- and temperature-induced changes in the birefringence. Three principle design techniques in the production of polarization conserving fibers have been attempted, with only

some degree of success. They are: (1) collapsed circular preform with cladding, (2) the use of preforms which permit the incorporation of a permanently-induced assymetric radial strain acting on the fiber core and (3) elliptical core fibers.

The nonconservation of polarization in an optical fiber, particularly if it is undergoing spontaneous changes, is equivalent to the presence of nonreciprocal random phase changes between the two counter-propagating waves traversing the interferometer. These nonreciprocal random phase changes (and hence, intensity fluctuations) are sources of optical noise in a fiber interferometer rotation sensor.

The experimental arrangement is shown in Figure 20. Light from a polarized Helium-Neon laser is passed through a polarizer in order to produce a very highly polarized source of radiation. The light is chopped by a mechanical chopper which also provides a reference signal to the lock-in amplifier. A half-wave plate w is used to adjust the polarization azimuth angle of the input light which is focused onto the fiber by a 20x microscope objective. The output light from the fiber is collimated by another 20x microscope objective and passed through a dichroic polarization analyzer A before being synchronously detected by a photodiode detector S and lock-in amplifier. A Babinet-Soleil compensator was inserted for accurate phase measurements between the two orthogonal polarization components.

The polarization measurements performed on the fibers were the polarization ratio R ($R = 20 \log_{10} \frac{I_{max}}{I_{min}}$), the azimuth angle of the output polarization ellipse and the relative phase difference between the two orthogonal modes of polarization. I_{max} and I_{min} are the intensities of the two polarization components.

Four different optical fibers were evaluated during the course of this work. Two of these fibers were used in working models of a fiber interferometer rotation sensor. These were the FIG and FROG systems. Both fibers were

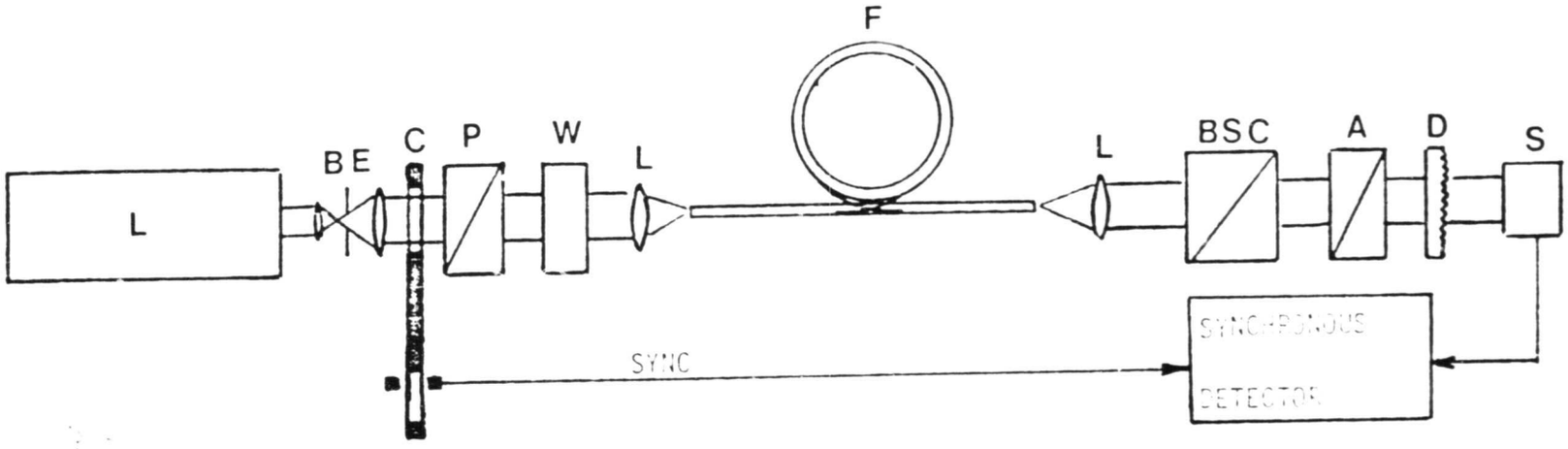

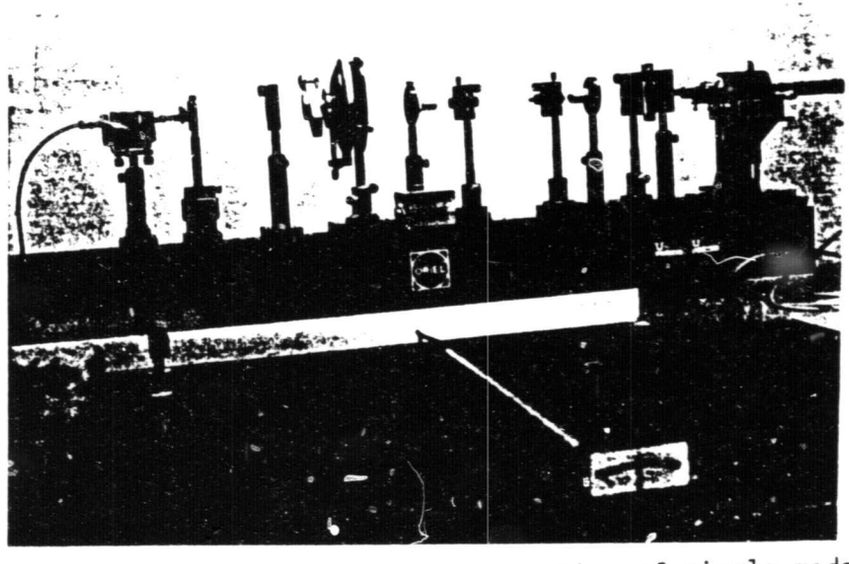

Figure 20. Experimental layout to evaluate polarization properties of single mode optical fibers. L = laser, BE = beam-expander, C = Mechanical Chopper, P = polarizer, W = $\lambda/2$ or $\lambda/4$ plates, L = focusing optics, F = fiber, BSC = Babinet-Soleil Compensator, A = analyzer, D = diffuser, S = Photodiode

manufactured by ITT, had lengths measuring 85 m and 1.57 km, and each had a core diameter of 4.5 μm. These fibers were snugly wound on cylinders having diameters of 0.26 m and 1.00 m, respectively. Two other fibers were also available for evaluation. These were small core fibers (2.4 μm) and were manufactured by ITT and FCI. The 30 m FCI fiber had no buffer or covering, was loosely wound on a 50 cm storage cylinder which hung from the laboratory ceiling. This fiber was very fragile, had no contact support and was simply allowed to droop on the optical table. The 10 m ITT fiber did have a RTV buffer and outer covering, as did the longer 85 m and 1.5 km fibers, although it tco was loosely wound (on the original shipping spool).

Figures 21-24 are plots of the polarization ratio R as a function of the azimuth angle of the input polarization vector. These results are in qualitative agreement with those of Ramaswamy, *et al.*[8]. In all four figures, the large polarization ratio corresponds to a polarization state that is very nearly linear (within the limits of source polarization). There are two such input azimuth angles, ninety degrees apart, for which the output is linearly polarized. This observtion is consistent with the fact that the fiber behaves, in some instances, like a simple birefringent wave-retarder.

However, all the fibers did not behave the same. Although the radiation exiting from the 30 m FCI fiber exhibited a high degree of polarization, there was a considerable amount of drift observed in the azimuth angle of the polarization vector for both input and output beams. This drift amounted to several tens of degrees over periods of 20-30 minutes. The primary source of this drifting was found to be due to changes in the thermal environment. Also, changes in the polarization state could be brought about by simply moving or touching the fiber lightly. The short 10 m ITT fiber (2.4 μm core) exhibited a similar behavior, although in that case a state of linear polarization could

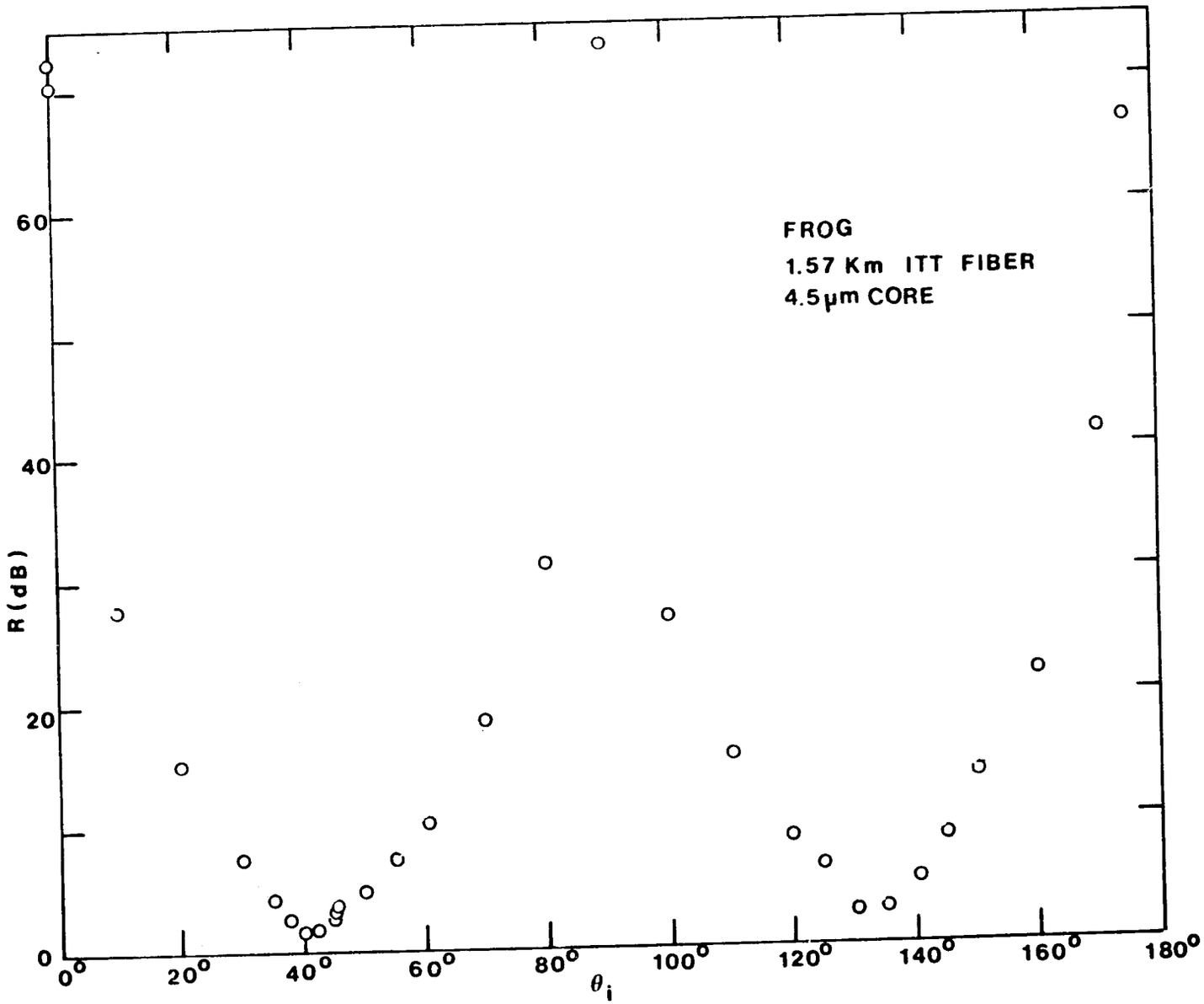

Figure 21. Polarization ratio R as a function of input polarization angle θ_i. The ratio R is defined by R = 20 $\log_{10}$(I max/I min).

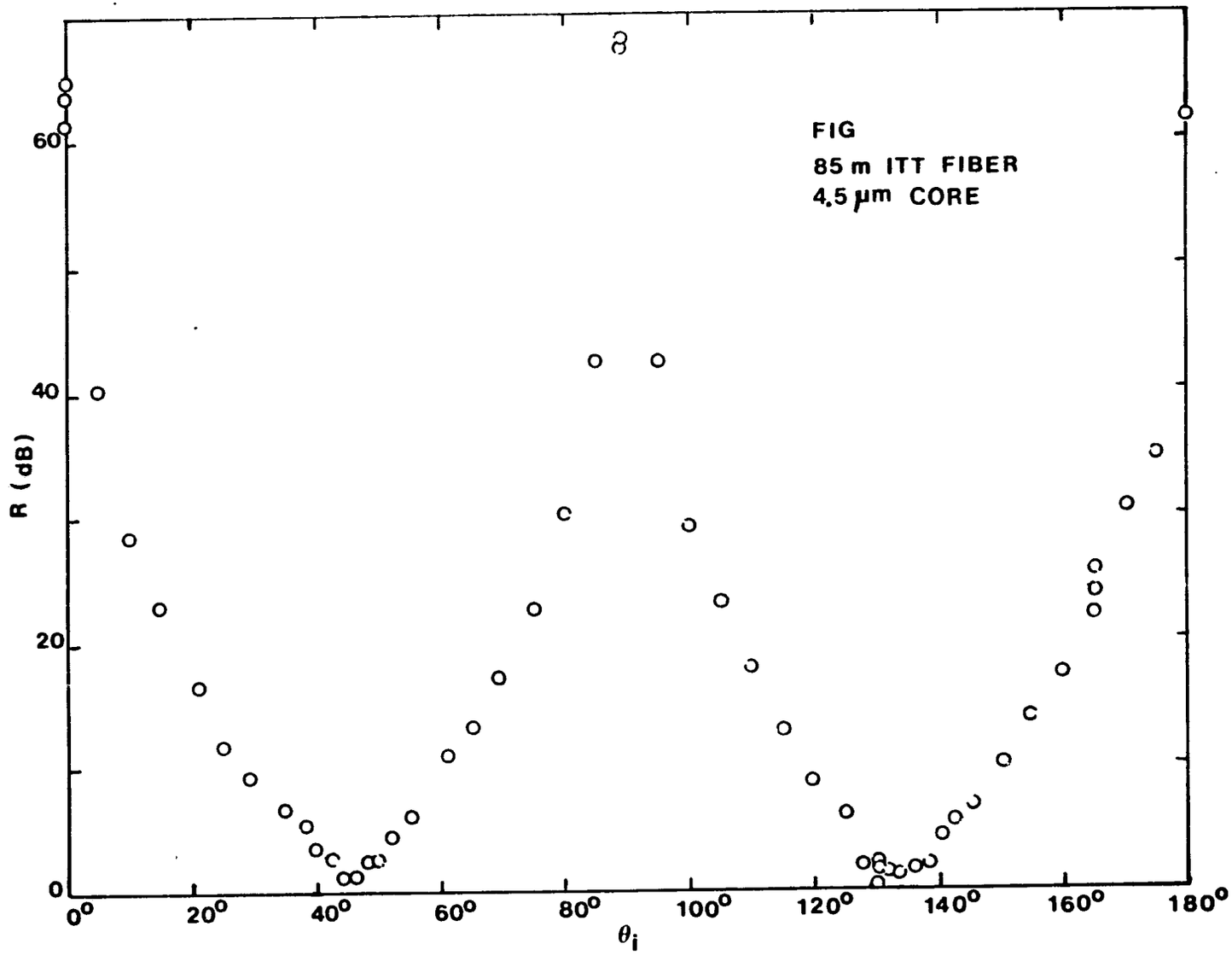

Figure 22. Polarization ratio R as a function of input polarization angle θ_i. The ratio R is defined by $R = 20 \log_{10} (\frac{I_{max}}{I_{min}})$.

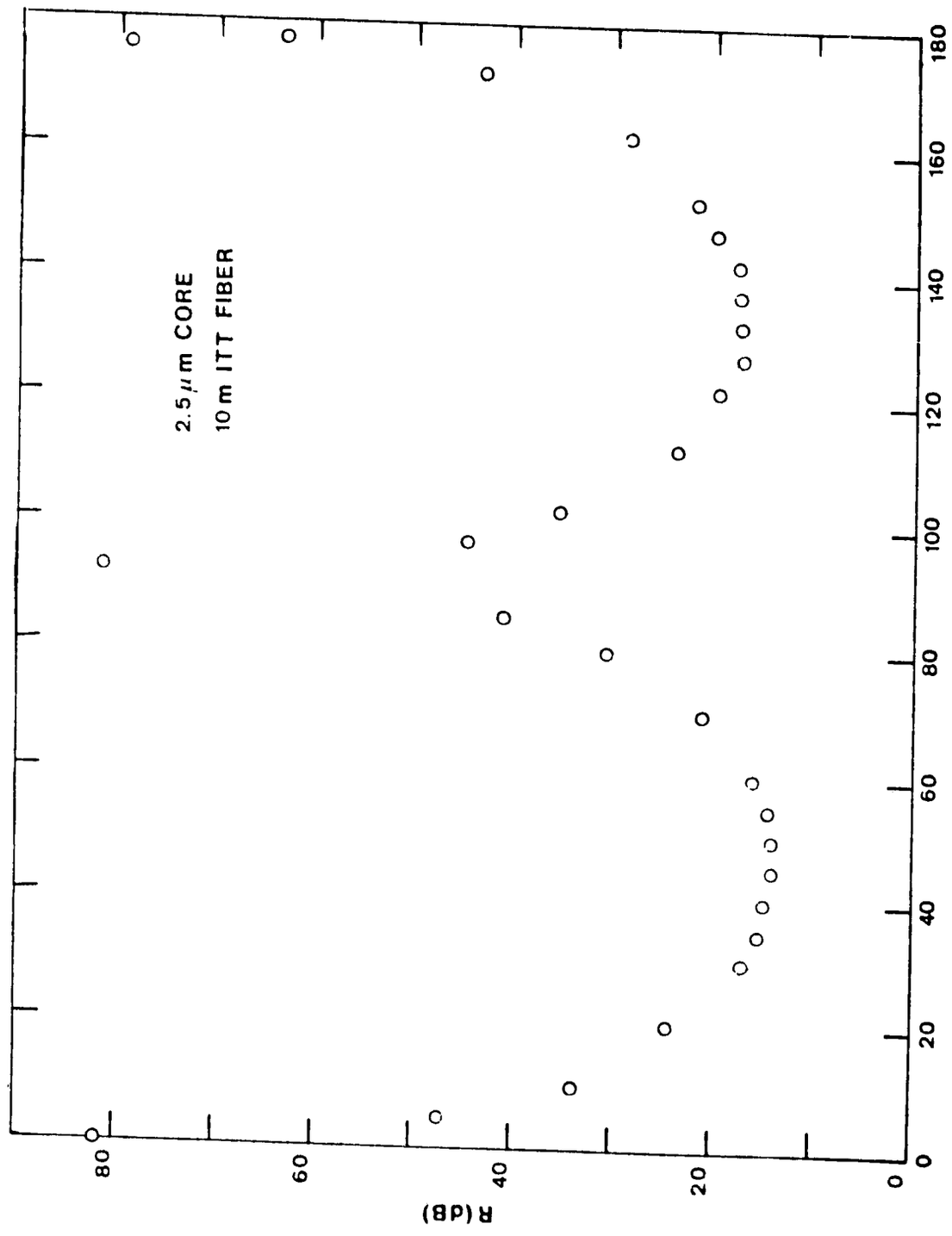

Figure 23. Polarization ratio R as a function of input polarization angle θ_i.

The ratio R is defined by $R = 20 \log_{10} \left(\frac{I_{max}}{I_{min}}\right)$.

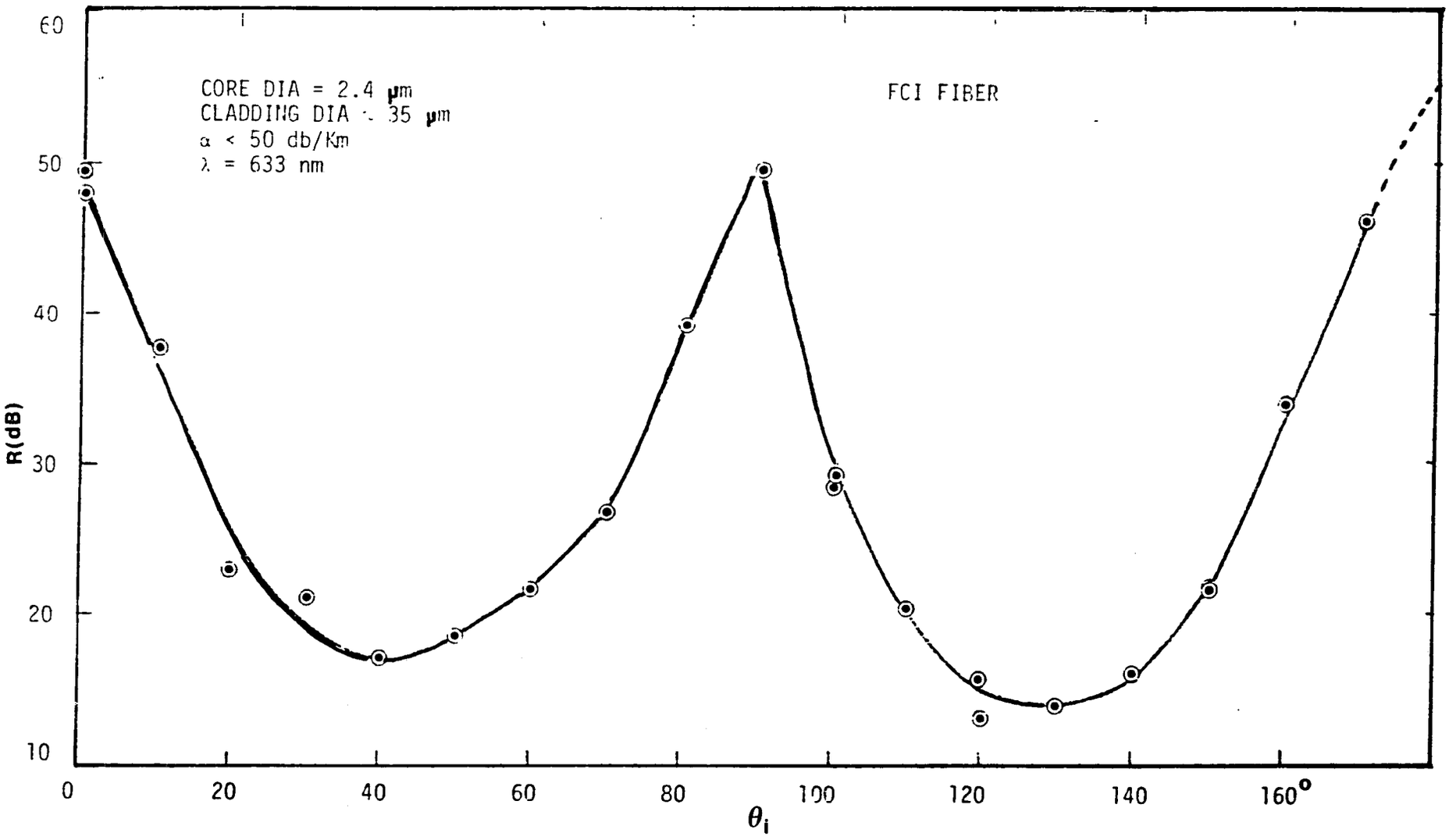

Figure 24. Polarization ratio R as a function of input polarization angle θ_i. The ratio R is defined by $R = 20 \log_{10} \left(\frac{I_{max}}{I_{min}}\right)$.

be preserved over longer periods of time (10's of minutes) without changing.

In contrast to the FCI fiber which had no buffer or covering and the 10 m ITT fiber which was wound loosely on the shipping spool, the 85 m and 1.57 km ITT fibers exhibited no measurable drifts in the polarization ratio for fixed input azimuth angles. In particular, the large polarization ratio observed when the input polarization vector was aligned parallel to one of the two principle axes of the fiber was maintained for a period of several weeks without any adjustment or alignment of the input azimuth angle. Thus, a state of linear polarization at the input could be preserved at the output over long periods of time. (Note: Although input and output polarization were highly linear, the polarization vectors were never parallel to one another and seemed to have preferential orientation with respect to the fiber coil.) This could be due to either twists in the fiber or optical activity.

The second type of measurement performed on these fibers was the relative orientation of the output polarization ellipse as a function of the input polarization angle. The results of these measurements are illustrated in Figures 25-28. The behavior of the FCI and 10 ITT fibers is similar to that observed at Bell Laboratories. These were loosely wound on a cylinder and the Bell Lab fibers were stretched out in a linear fashion. The correlation between the input and output polarizations for the 85 m and 1.57 km ITT fibers, snugly wound in coil forms about cylinders, is distinctly different from that of the loosely wound fibers. It is seen in Figures 25 and 26 that the output azimuth angle is somewhat independent (although never completely) of the input polarization vector alignment until it approaches 45° (or a suitable odd multiple). At this point, the orientation of the output ellipse changes dramatically (almost 90°). This behavior does not seem to be typical of that expected if we were to treat the fiber as a simple birefringent wave-retarder since a smoother

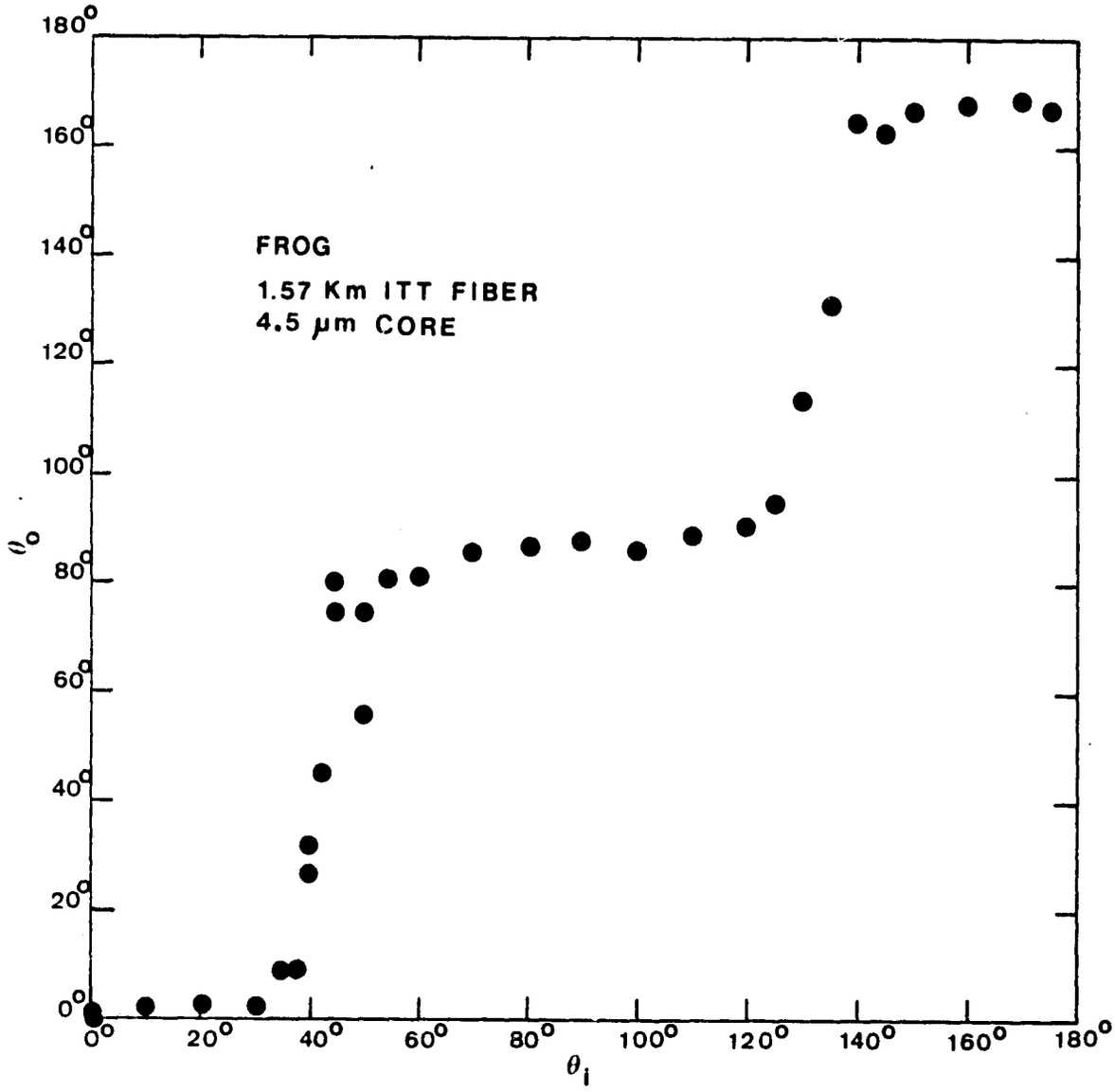

Figure 25. Orientation of the polarization ellipse θ_o as a function of input angle θ_i. The fiber is in the form of a ring one meter in diameter, core diameter 4.5 μm, cladding diameter 83 μm, optical attenuation 8 dB/km and the source wavelength 633 nm.

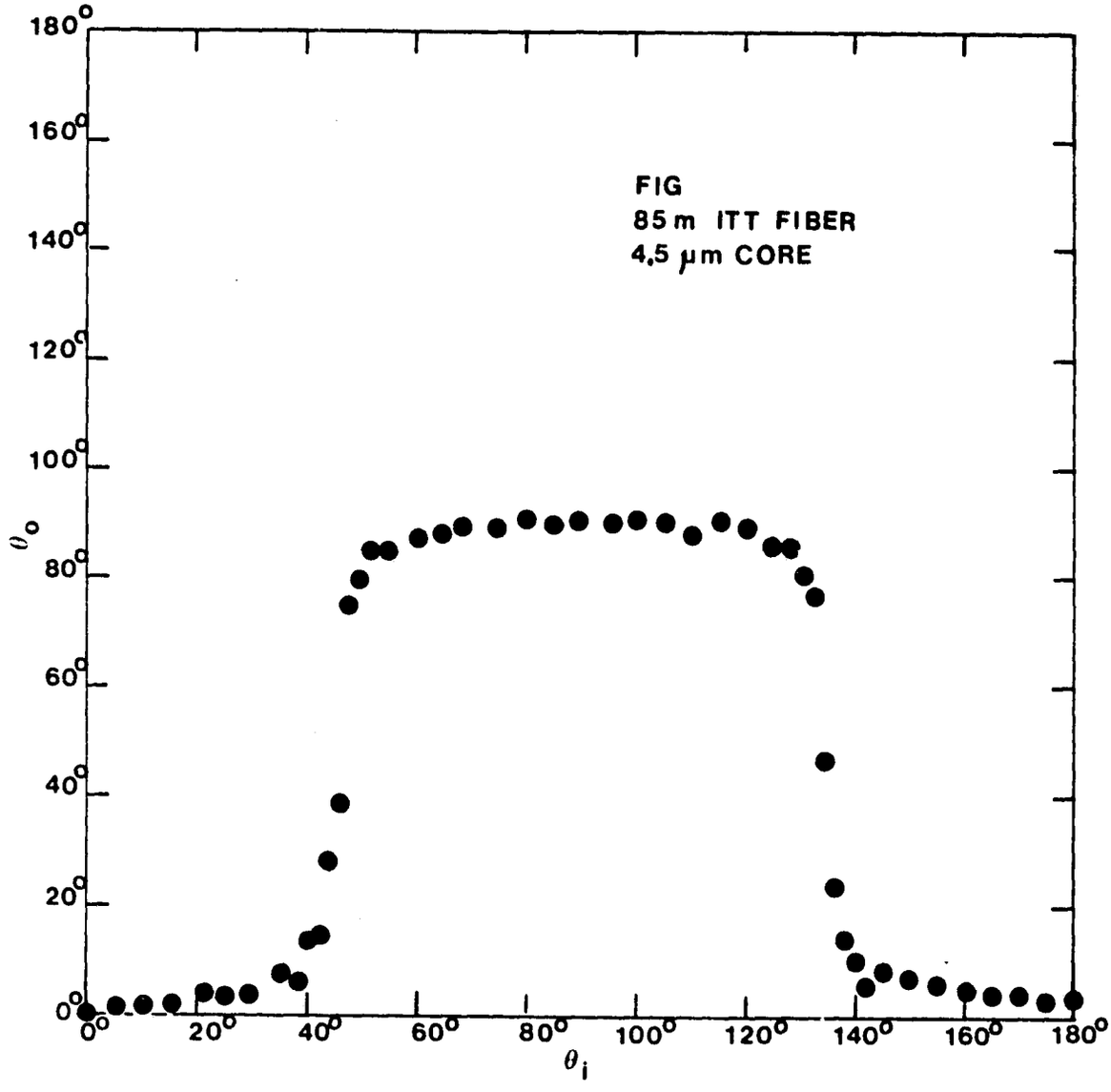

Figure 26. Orientation of polarization ellipse θ_o as a function of input angle θ_i. The fiber is in the form of a ring 52 cm in diameter, core 4.5 μm, cladding diameter 83 μm, optical attenuation 17 dB/km and the source wavelength 633 nm.

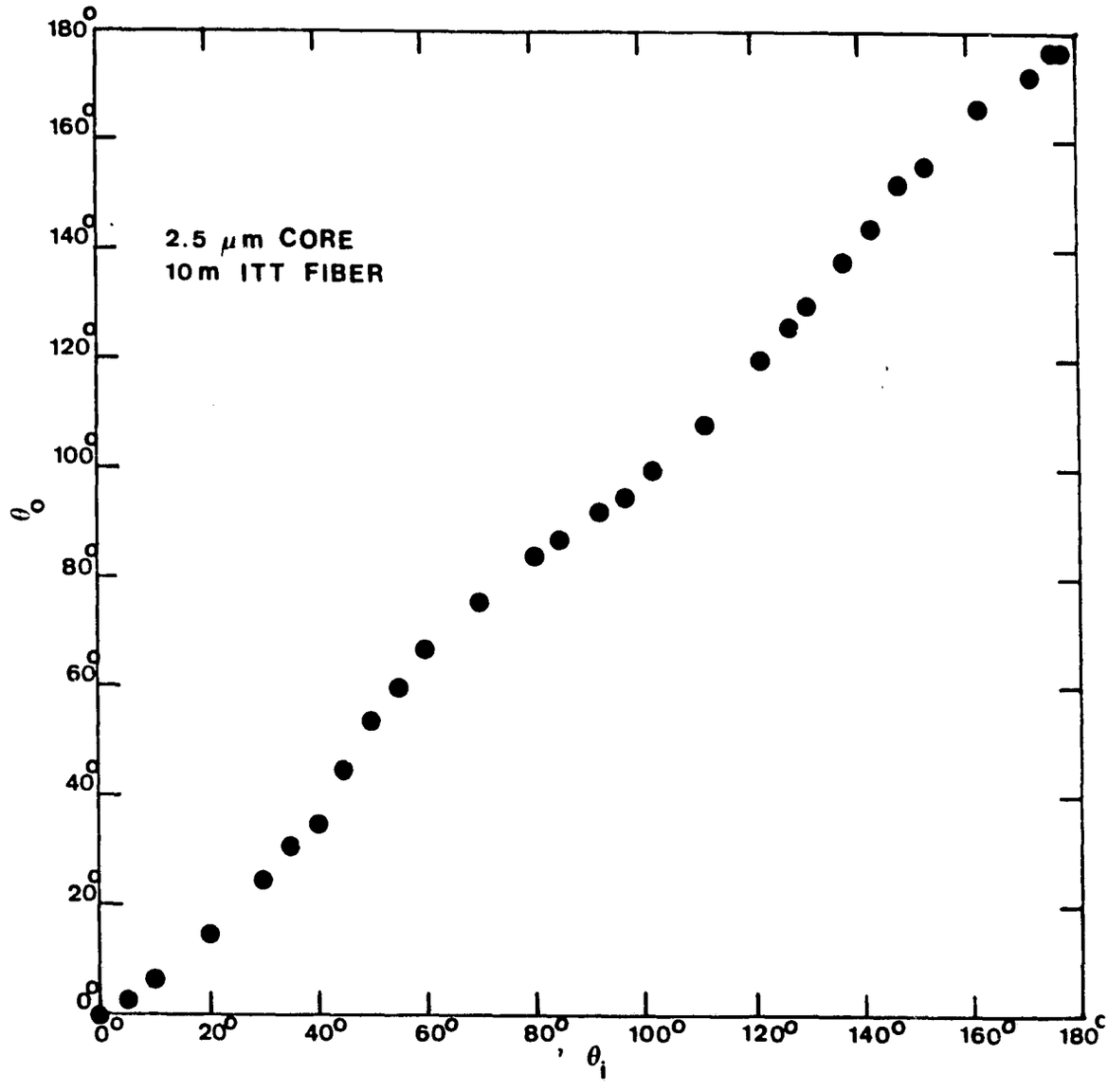

Figure 27. Orientation of the polarization ellipse θ_o as a function of input angle θ_i.

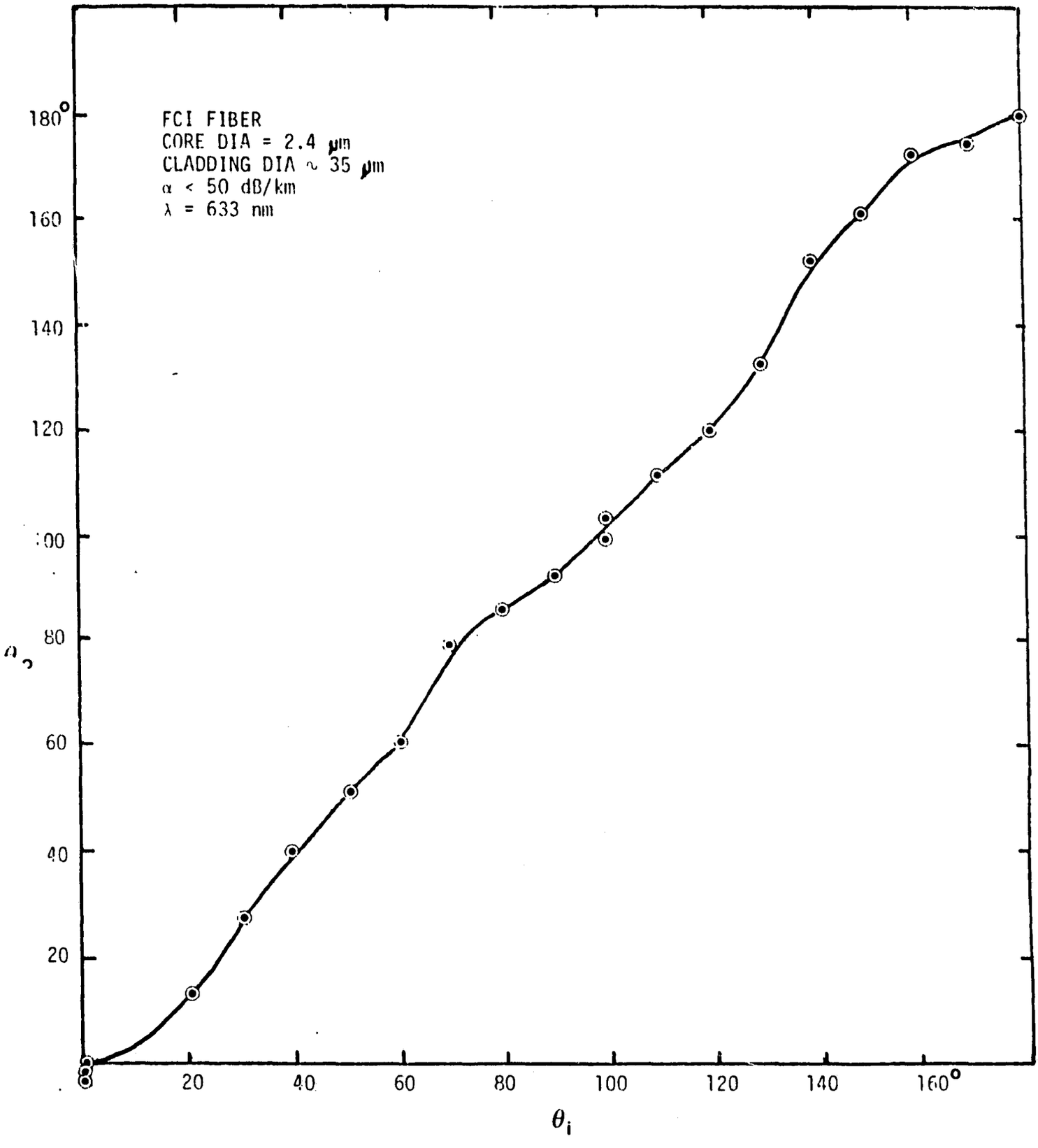

Figure 28. Orientation of the polarization ellipse θ_o as a function of input angle θ_i.

transition would be expected. Clearly, this departure is somehow related to the wave-guiding properties of the fiber.

Another matter of potential concern was the observation of a relatively strong time-dependent coupling that existed between the two orthogonal modes of polarization whenever the input radiation was coupled into the fiber with the polarization vector approximately 45° to the principal axes of the fibers. The coupling was confirmed by the observation of the intensity changes in either of the two orthogonal modes of polarization. This suggests that great care must be exercised in the coupling of the laser beam into the fiber since these intensity fluctuations can be interpreted as phase fluctuations induced by rotation (i.e., a gyroscope operating in this mode would have a high "drift-rate" error).

The last type of measurement performed was that of the relative phase difference between the two polarization modes (using the Babinet-Soleil compensator) for each of the two longer fibers. In both instances, the phase difference amounted to approximately 1.4 λ, consistent with the minimum polarization ratio R.

4.0 CONCLUSIONS

It was the goal of this research project to evaluate the fiber ring optical gyroscope in terms of noise sources, particularly optical. A one meter diameter ring with about 1600 meters was constructed. To eliminate reflections from the fiber end, the optics, detectors, and fiber holders were immersed in a matching fluid. This reduced the end reflections significantly. However, this was not as successful with the other optical surfaces and reflections were still present. Thermal variations in the fluid and electronic noise prevented the detection of earth rotation rate with the FROG I system (DC detection). Even with the synchronous detection system and subsequent improvement of the electronic design (FROG II), thermal drifts were still a serious problem (see Figure 29). The diode laser was used in place of the HeNe laser, but reflections from the fiber ends and other surfaces were a serious problem (see Figure 30). No further work with the diode laser was done. Further configuration suggestions for the FROG are shown in Figure 29.

The final conclusion from the FROG study is that a discrete system has very serious limitations. Not only were there optical noise sources which were hard to control, but thermal and mechanical stability requirements could not be met with the configuration used. Modulation techniques were not investigated as shown in Figure 29 (FROG IV and FROG V). McLandrich and Rast[9] at NOSC have built and tested a system similar to FROG IV which operated successfully very close to earth rate but had some of the same problems that were encountered with FROG I and II.

Many of the problems could be avoided with an all integrated optic approach, with the laser source, modulator, detector, beamsplitter, bias element, etc., on a single chip[10,11].

We recommend that development of integrated optic components be encouraged. In the initial stages, perhaps only individual functions would be developed (i.e., beamsplitter/modulator) while the laser source and detector would be discrete as before.

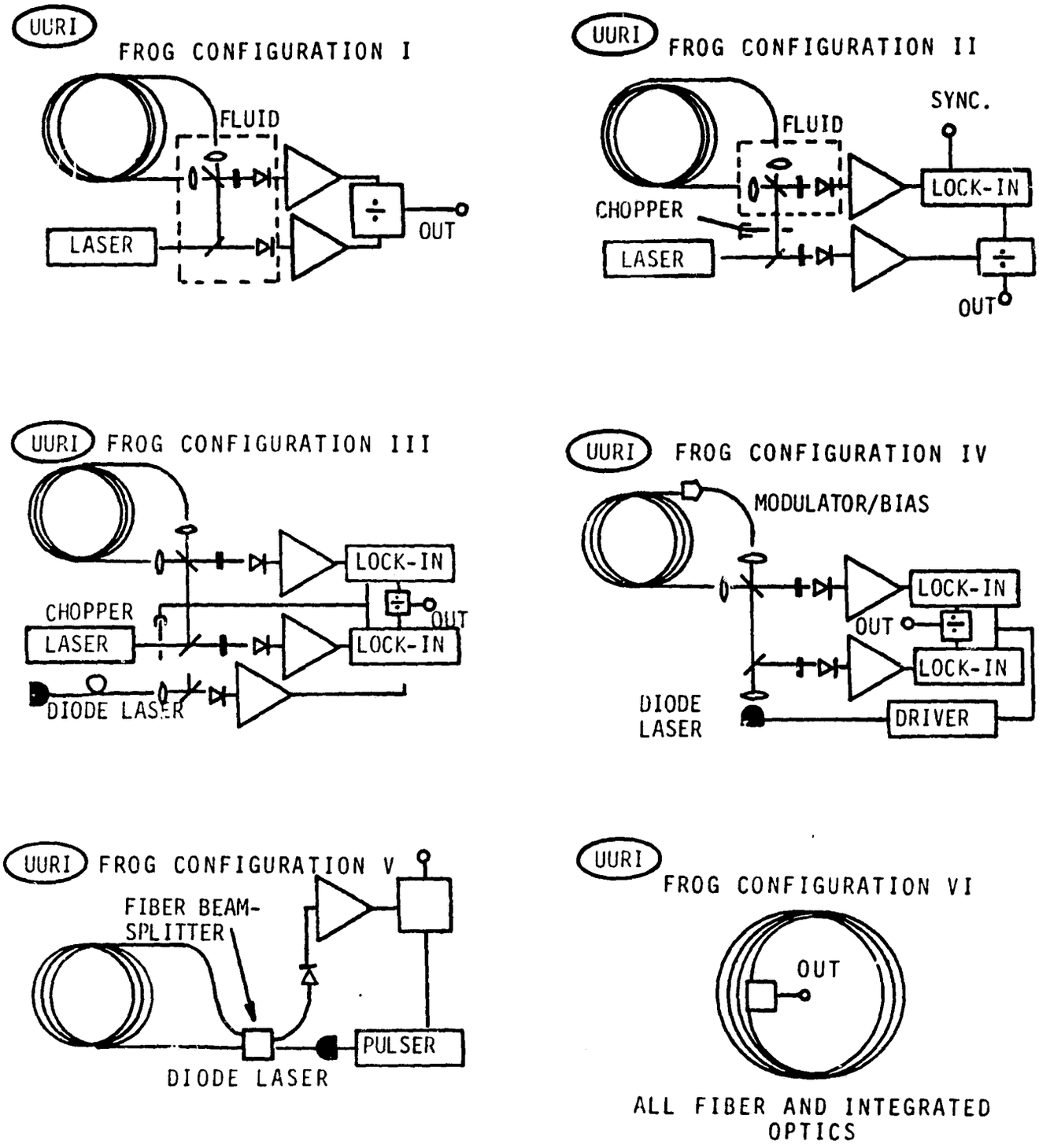

Figure 29. Various proposed configurations of the FROG.

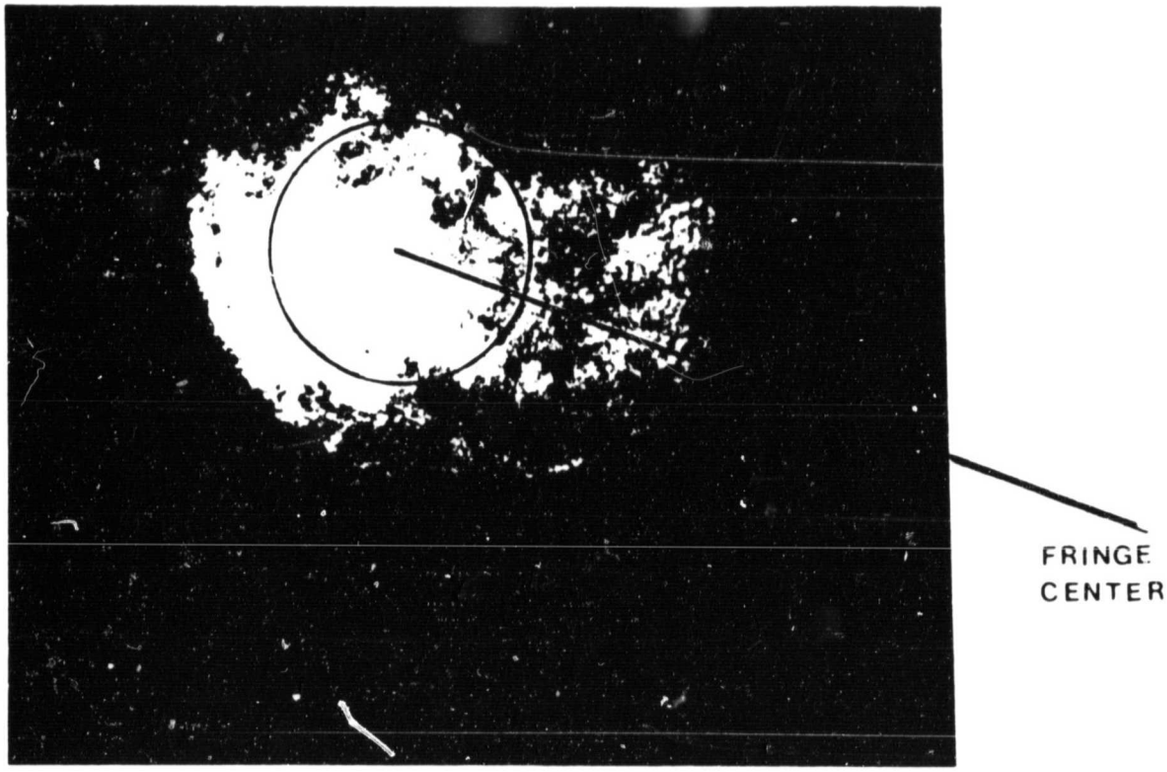

Figure 30. Photograph of fringe patterns produced with a diode laser. The fiber ends were in air.

5.0 REFERENCES

1) Sagnac, G. (1913), Comptes Rendus 157, 708.

2) Pogany, B., (1926), Ann. Physik 80, p. 217. See also Pogany, B. (1928). Ann. Physik 85, 244.

3) Michelson, A. A. and Gale, H. G. (1925), Astrophys. Jour, 61, 140.

4) Post, E. J. (1967). Rev. of Mod. Phy. 39, 475.

5) Vali, V. and Shorthill, R. W., (1976). Appl. Optics 15, No. 5, 1099.

6) Vali, V. and Shorthill, R. W. (1977). Appl. Optics 16, No. 2, 290.

7) Vali, V. and Shorthill, R. W., and Berg, M. F. (1977). Final Report NASA Contract NASW 2967. Geospace Sciences Laboratory Publication 77-008. Univ. Utah Research Institute, Salt Lake City, Utah.

8) Ramaswamy, V., Standley, R. D., Sze, D. and French, W. G. (1978). The Bell Sys. Tech. J. 57, No. 3, 635.

9) McLandrich and Rast, H. E. (1978). Proceedings SPIE 57 127 (August 30-31, 1978, San Diego, CA).

10) Goss, W. C., Goldstein, R., Nelson, M. D. and Fearnehaugh, H. T. (1980), "Fiber Optic Rotation Sensor Technology". Appl. Optics (March).

11) Papuchon, M. and Puech, C. (1978), "Integrated Optics - A Possible Solution For Fiber Gyroscopes", Proceedings SPIE 157, 218 (August 30-31, 1978, San Diego, CA).

6.0 APPENDICES

A. Measurements of V. Vali and M. F. Berg

This paper was published in the proceedings of SPIE. The paragraphs marked with asteriks were completed more than four months after the authors were no longer in the employment of the University of Utah Research Institute.

B. Presentations, Seminars, Published Papers

A list of presentations, seminars, and published papers are listed below:

1. "Fiber Gyroscopes", V. Vali and M. F. Berg, SPIE talk given August 31, 1978, Session 11, Laser Inertial Rotation Sensors, Town and Country Motel, San Diego, California. Presented by V. Vali.

2. ONR Workshop, "Optical Fiber Gyroscopes Theory" presented by V. Vali, and the "Experimental Results" obtained at the Geospace Sciences Laboratory presented by R. W. Shorthill.

3. "Optical Fiber Gyroscope", R. W. Shorthill, G. J. Morris, L. D. Weaver. Presented at IFAC Conference, Oxford, England, July 2-6, 1979. VIII IFAC Symposium on Automatic Controls in Space presented by R. W. Shorthill.

4. Various presentations and descriptions of the work in progress were briefly reported in proposals made to potential sponsors.

NONRECIPROCITY NOISE IN FIBER GYROSCOPES AND MEASUREMENT OF FIBER DISPERSION

V. Vali and M. F. Berg*
University of Utah Research Institute
Salt Lake City, Utah 84108

It has been shown previously (1) that the dispersion term in the Fresnel drag coefficient can be detected using a moving single mode fiber as the beam path. This letter reports on the results of a study of optical noise sources in fiber gyroscopes as well as on determining the dispersion term with higher accuracy.

The fringe shift ΔZ in a fiber ring interferometer is:

$$\Delta Z = \frac{2\omega LR}{\lambda C} n^2(1-\alpha)\cos\theta \qquad (1)$$

where ω is the angular velocity, L is the fiber length, R is the fiber coil radius, λ is the free space wavelength of light, C is the free space velocity of light, n is the index of refraction of the fiber, α is the Fresnel drag coefficient, and θ is the angle between the fiber coil axes and the rotation axes. The Fresnel drag coefficient is:

$$\alpha = 1 - \frac{1}{n^2} - \frac{\lambda}{n}\frac{dn}{d\lambda} \qquad (2)$$

The last term in this expression is the dispersion term.

In this experiment the fiber coil was mounted on a Genesco rate table (Model C-181). The angle between the rate table rotation axes and the fiber coil axes was made equal to the latitude of Salt Lake City - 40.74°.

The fiber coil was made such that when the fiber was layer wound (10 layers) the average fiber loop diameter was 100 $\pm$ 0.05 cm. The deviation from a circle was less than 0.1 cm. A total of 500 full turns of fiber was used. The geometry of connecting the fiber ends to the interferometer components that were located in the center of the fiber coil, added another 0.3 turns to the coil. Therefore, L = 1571.7 $\pm$ 0.3 meters. The fiber was made by ITT and has an attenuation of about 8 dB/km at λ = 6328 Å. Its core diameter is 5.5 μm. A Spectra Physics HeNe laser (Model 138P) was used as the light source.

To eliminate the optical noise associated with fiber end reflections (and reflections from other optical components) the interferometer parts including the fiber ends were immersed in index matching fluid. Without this precaution the extra fringe patterns that are formed between the fiber ends, the cube beam splitter sides and fiber ends, etc. would have caused intensity fluctuations in the center of the circular fringe pattern that are equivalent to a large fraction of a fringe.

To measure the fringe shift ΔZ as a function of the angular velocity ω, the ratio of photocurrents at the center of the circular fringe pattern and the direct laser light was recorded. The angular velocity of the fiber coil was increased in increments of about 1 deg/sec. The rotation velocity was varied between 0 deg/sec. and 115 deg/sec. A section of such a recording is shown in Figure 1. For the calibration of this fiber interferometer gyroscope, eleven complete fringes were used. The result is:

9.20 ± 0.01 deg/sec/fringe

The largest uncertainty of this study arose from the nonreciprocal effects caused by variations in the elasto-optically induced optical activity and linear birefringence. (2) The magnitude of this variation changed the apparent fringe phase by about 5% of the distance between fringes. This effect is seen in Figure 1 as the apparent intensity fluctuation when the angular velocity is kept constant.

Using equation (1) and n = 1.457, one gets:

$$\alpha = 0.5324 \pm 0.0005$$

and from equation (2):

$$\frac{dn}{d\lambda} = -(7.9 \pm 1.0)\cdot 10^{-5}\ \text{Å}^{-1}$$

This dispersion is about a factor of 3 smaller than the value of material dispersion for bulk fused quartz. The reduction is presumably due to the effect of waveguide dispersion (which has the opposite sign of the material dispersion) since the fringe position depends on the total dispersion.

* When the rate table is rotated around the local vertical axes, the angular relationship between the fiber gyro sense coil axes and the earth's rotation axes varies in such a way as to be alternately parallel and perpendicular. Since the instrument measures the vector

* Vali and Berg are presently at Rockwell International, 3370 Miraloma Ave, Anaheim, CA 92803

sum of these two rotations, the observed fringe shift is composed of a small sinusoidally varying fringe shift (produced by earth rotation) added to a constant fringe shift produced by the rate table rotation.

* Since Salt Lake City is not at the 45° parallel, but is located at 40.7° north latitude, the instrument was constructed so that the fiber gyro sense coil axis would become perpendicular to the earth's rotation axes during rotation of the rate table, and therefore could not become completely parallel to the earth rotation axes. Therefore, only 98.9% of the maximum additional fringe shift due to earth rotation was obtained.

* To average the optical path nonreciprocity noise, the table was rotated at about 80 deg/sec. for 20 minutes. The ratio of photodetector outputs was recorded. At the beginning of each revolution, the scope was triggered. The result is shown in Figure 2. The earth rotation contribution amounts to about 1.5 small scale divisions. It is just observable within the random fluctuations in the fringe position as caused by the birefringence.

Therefore, at present the variations in the optical path nonreciprocity of the fiber limit the accuracy of the fiber ring interferometer gyroscope to about 10 times the earth rotation rate.

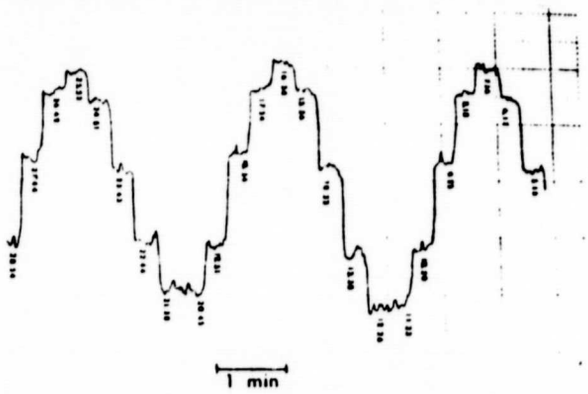

Figure 1

A section of recording the fringe shift as a function of the rotation velocity. The angular velocity in degrees per second is indicated on the recording. The optical nonreciprocity noise is seen as the apparent fringe position fluctuation as the angular velocity is kept constant.

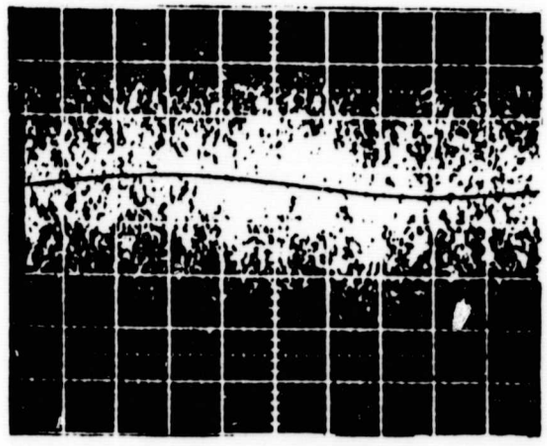

* Figure 2

A photographic integration of the fringe position at an angular velocity of about 80 deg/sec. The scope was triggered at the beginning of each revolution. About 300 revolutions were recorded. The large fluctuations of the fringe position were due to variations in optical nonreciprocity. The calculated contribution of earth rotation is indicated by the black line.

References

1. V. Vali, R. W. Shorthill and M. F. Berg, Appl. Opt. 16, 2605 (1977).

2. R. Ulrich and A. Simon, Polarization Optics of Twisted Single-Mode Fibers, to be published in Applied Optics.